



Deposited via The University of Leeds.

White Rose Research Online URL for this paper:

<https://eprints.whiterose.ac.uk/id/eprint/116453/>

Version: Accepted Version

Article:

Mishra, B, Shoenfelt, E, Yu, Q et al. (2017) Stoichiometry of mercury-thiol complexes on bacterial cell envelopes. *Chemical Geology*, 464. pp. 137-146. ISSN: 0009-2541

<https://doi.org/10.1016/j.chemgeo.2017.02.015>

(c) 2017 Published by Elsevier B.V. This manuscript version is made available under the CC BY-NC-ND 4.0 license <http://creativecommons.org/licenses/by-nc-nd/4.0/>

Reuse

Items deposited in White Rose Research Online are protected by copyright, with all rights reserved unless indicated otherwise. They may be downloaded and/or printed for private study, or other acts as permitted by national copyright laws. The publisher or other rights holders may allow further reproduction and re-use of the full text version. This is indicated by the licence information on the White Rose Research Online record for the item.

Takedown

If you consider content in White Rose Research Online to be in breach of UK law, please notify us by emailing eprints@whiterose.ac.uk including the URL of the record and the reason for the withdrawal request.

1 **Stoichiometry of mercury-thiol complexes on bacterial cell envelopes**

2
3 **Bhoopesh Mishra^{1*†}, Elizabeth Shoenfelt², Qiang Yu³, Nathan Yee⁴,**

4 **Jeremy B. Fein³, Satish C.B. Myneni^{2*}**

5
6 ¹Physics Department, Illinois Institute of Technology, Chicago, Illinois, USA

7 ²Department of Geosciences, Princeton University, Princeton, New Jersey, USA

8 ³Department of Civil Engineering & Geological Sciences, University of Notre Dame, Notre Dame,
9 Indiana, USA

10 ⁴Department of Environmental Sciences, Rutgers University, New Brunswick, New Jersey, USA

11
12
13 Keywords: Hg, speciation, stoichiometry, bacteria, thiols, XANES, EXAFS, cell envelope,
14 potentiometric titration, qBBR

15
16
17
18
19
20
21
22
23
24 _____
25 *Co-corresponding authors. Email: (bmishra3@iit.edu); (smyneni@princeton.edu)

26 †Present address: School of Chemical and Process Engineering, University of Leeds, Yorkshire, UK.
27
28
29

30 Abstract

31 We have examined the speciation of Hg(II) complexed with intact cell suspensions (10^{13}
32 cells L^{-1}) of *Bacillus subtilis*, a common gram-positive soil bacterium, *Shewanella oneidensis*
33 MR-1, a facultative gram-negative aquatic organism, and *Geobacter sulfurreducens*, a gram-
34 negative anaerobic bacterium capable of Hg-methylation at Hg(II) loadings spanning four orders
35 of magnitude (120 nM to 350 μ M) at pH 5.5 (± 0.2). The coordination environments of Hg on
36 bacterial cells were analyzed using synchrotron based X-ray Absorption Near Edge Structure
37 (XANES) and Extended X-ray Absorption Fine Structure (EXAFS) spectroscopy at the Hg L_{III}
38 edge. The abundance of thiols on intact cells was determined by a fluorescence-spectroscopy
39 based method using a soluble bromobimane, monobromo(trimethylammonio)bimane (qBBr) to
40 block thiol sites, and potentiometric titrations of biomass with and without qBBr treatment. The
41 chemical forms of S on intact bacterial cells were determined using S k-edge XANES
42 spectroscopy.

43 Hg(II) was found to complex entirely with cell bound thiols at low Hg:biomass ratios.
44 For *Bacillus subtilis* and *Shewanella oneidensis* MR-1 cells, the Hg-S stoichiometry changed
45 from Hg-S₃ to Hg-S₂ and Hg-S (where 'S' represents a thiol site such as is present on cysteine)
46 progressively as the Hg(II) loading increased on the cells. However, *Geobacter sulfurreducens*
47 did not form Hg-S₃ complexes. Because the abundance of thiol was highest for *Geobacter*
48 *sulfurreducens* (75 μ M/g wet weight) followed by *Shewanella oneidensis* MR-1 (50 μ M/g wet
49 weight) and *Bacillus subtilis* (25 μ M/g wet weight), the inability of Hg(II) to form Hg-S₃
50 complexes on *Geobacter sulfurreducens* suggests that the density and reactivity of S-amino acid
51 containing cell membrane proteins on *Geobacter sulfurreducens* are different from those of
52 *Bacillus subtilis* and *Shewanella oneidensis* MR-1. Upon saturation of the high affinity thiol sites
53 at higher Hg:biomass ratios, Hg(II) was found to form a chelate with α -hydroxy carboxylate
54 anion. The stoichiometry of cell envelope bound Hg-thiol complexes and the associated
55 abundance of thiols on the cell envelopes provide important insights for understanding the
56 differences in the rate and extent of uptake and redox transformations of Hg in the environment.

57

58

59

60

61

62

63

64

65

66 1.0 Introduction

67 Mercury is a common contaminant found in many terrestrial and aquatic systems, and its
68 bioaccumulation in organisms, including humans, is a major environmental concern (Mergler et
69 al, 2007). The solubility, speciation, toxicity and the ultimate fate of Hg within aquatic
70 ecosystems is dependent on a large number of chemical and biological variables (Morel et al.,
71 1998; Barkay and Schaefer, 2001). In aquatic systems, Hg solubility is high under oxygen-rich
72 acidic conditions but it is significantly inhibited under anoxic sulfide-rich waters (Martell and
73 Smith, 1974). The Hg-sulfide complexes are among the strongest complexes of all known Hg
74 inorganic and organic complexes in the aquatic environment (Carty and Malone, 1979). While
75 the presence of sulfides in aqueous systems can induce precipitation of Hg in the form of
76 insoluble amorphous and crystalline HgS, stable aqueous polysulfide complexes and
77 nanoparticles can also enhance the solubility and transport of Hg. In addition, inorganic ligands
78 (e.g. Cl⁻), and mono- (e.g. cysteine) and poly-dentate (e.g. citrate, catechols) organic ligands can
79 also enhance the solubility of Hg by forming stable aqueous complexes. Complex organic
80 ligands, such as natural organic matter (NOM), also form stable Hg-NOM complexes through
81 thiol (SH), and carboxyl binding (Xia et al., 1999; Haitzer et al., 2002; Khwaja et al., 2006;
82 Skyllberg et al., 2005; Skyllberg 2008; Nagy et al., 2011; Hesterberg et al., 2001). Because
83 dissolved organic matter (DOM) is the main source of reduced cysteine residues in natural
84 waters, Hg complexation with DOM is thought to control the speciation, solubility, mobility, and
85 toxicity of Hg in the aquatic environment (Loux, N., 1998; Ravichandran, M., 2004), indirectly
86 affecting the rate and extent of Hg-methylation (Ravichandran, M., 2004).

87 One of the key biogeochemical transformations of interest is the role of microorganisms
88 in converting Hg to methyl mercury. While the geochemical factors that control Hg methylation
89 in terrestrial and aquatic systems are poorly understood, it has been shown that the concentration
90 of Hg bioavailable to Hg-methylating bacteria is strongly affected by binding to cysteine
91 residues (Skyllberg et al., 2006), and the extent of Hg(II) uptake and Hg-methylation is
92 significantly influenced by the presence of Hg-cysteine complexes in aqueous solutions
93 (Schaefer and Morel, 2009; Schaefer et al., 2011; Thomas et al., 2014; Lin et al., 2015).

94 Thiol sites within bacterial cell envelopes have been shown to control the fate and
95 transport of Hg by providing high-affinity binding sites (Mishra et al., 2011), and mediating
96 redox transformations (Colombo et al., 2013; Hu et al., 2013; Colombo et al., 2014). Certain
97 bacterial strains such as *Geobacter sulfurreducens* PCA can function both as a reductant and as
98 an adsorbent for Hg(II) at different cell biomass to Hg ratios (Hu et al., 2013), with adsorption
99 being the dominant mechanism at low Hg:biomass ratios. Sorption of Hg(II) to cell envelope
100 sites has been thought to serve as a “sink” for Hg(II) that restricts transport into the cytoplasm,
101 thus lowering the bioavailability of Hg(II) (Graham et al., 2012). Recent studies indicate that in
102 addition to gene expression and regulation, cell envelope chemistry is likely an important driver
103 for cross-species differences in Hg methylation rates (Graham et al., 2012). Furthermore,
104 reactivity of thiols towards Hg(0), resulting in thiol mediated passive microbial oxidation of
105 Hg(0), has been recently reported (Colombo et al., 2013; Colombo et al., 2014). Since
106 physicochemical sorption of Hg(0) to reactive thiol sites has been hypothesized as the first step
107 in Hg(0) oxidation by dissolved organic matter (Gu et al., 2011; Zheng et al., 2012), differences
108 in passive Hg(0) oxidation rates by different bacterial strains could be explained by the reactivity

109 and density of thiols present on the cell envelopes of corresponding bacterial strains (Colombo et
110 al., 2014).

111 In spite of the significance of Hg-thiol complexation on cell envelopes, the speciation and
112 stability of thiol-bound Hg on cell envelopes remains largely unknown. X-ray-based
113 spectroscopy investigations could provide definitive information regarding the nature of Hg(II)
114 interactions with bacterial cell envelopes. To date, studies have been primarily limited to
115 showing the complexation of Hg with high (thiol) and low (carboxyl) affinity sites on cell
116 envelopes (Mishra et al., 2011; Dunham-Cheatham et al., 2014; Dunham-Cheatham et al., 2015).
117 Although recent studies have shown variations of the stoichiometry of thiol bound Hg on the
118 cell, they are either qualitative using a XANES fingerprinting technique (Thomas et al., 2014) or
119 limited in scope (Thomas et al., 2016). Similar to the complexation of Hg with NOM, Hg-thiol
120 complexes within bacterial cell envelopes may exhibit a range of stoichiometries as a function of
121 Hg loading conditions. The speciation and stability of such cell envelope bound Hg-thiol
122 complexes may in fact control the overall fate and bioavailability of Hg in aquatic systems. This
123 study provides direct evidence for systematic changes in the stoichiometry of Hg-thiol
124 complexes on bacterial cell envelopes for three different bacterial species.

125 For an in-depth evaluation of the speciation of Hg bound to cell envelopes and the
126 stoichiometry of Hg-thiol complexes under ambient conditions, we selected three distinct classes
127 of bacteria: *Bacillus subtilis*, a common Gram-positive soil bacterium, *Shewanella oneidensis*
128 MR-1, a facultative Gram-negative aquatic organism, and *Geobacter sulfurreducens*, a Gram-
129 negative anaerobic bacterium capable of methylating mercury; and exposed the intact cell
130 suspensions (10^{13} cells L⁻¹, or ~2 g L⁻¹ of wet mass) to different concentrations of dissolved
131 Hg(II) (120 nM to 350 μ M) at pH 5.5 (\pm 0.2). The structure and coordination environments of Hg
132 on the bacterial cells were analyzed using synchrotron-based X-ray Absorption Near Edge
133 Structure (XANES), and Extended X-ray Absorption Fine Structure (EXAFS) spectroscopy at
134 the Hg L_{III} edge. The abundance of thiols on the intact cells was directly determined by a
135 fluorescence-spectroscopy-based method, using a soluble bromobimane,
136 monobromo(trimethylammonio)bimane (qBBr), and was further verified by the change in total
137 thiol concentrations on intact cells using potentiometric titrations of biomass with and without
138 qBBr treatment. The chemical forms of S on intact bacterial cells were determined using S k-
139 edge XANES spectroscopy.

140 **2.0 Materials and Methods**

141 *2.1 Bacterial Growth Conditions*

142 *Bacillus subtilis* and *Shewanella oneidensis* MR-1 cells were cultured and prepared
143 aerobically following the procedures outlined elsewhere (Borrok et al., 2007). Briefly, cells were
144 maintained on agar plates consisting of trypticase soy agar with 0.5% yeast extract added. Cells
145 for all experiments were grown by first inoculating a test-tube containing 3 mL of trypticase soy
146 broth with 0.5% yeast extract, and incubating it for 24 h at 32 °C. The 3 ml bacterial suspension
147 was then transferred to a 1 L volume of trypticase soy broth with 0.5% yeast extract for another
148 24 h on an incubator shaker table at 32 °C. Cells were pelleted by centrifugation at 8100g for 5
149 min, and rinsed 5 times with 0.1 M NaClO₄.

150 *Geobacter sulfurreducens* cells were cultured and prepared using a different procedure
151 than described above. Cells were maintained in 50 mL of anaerobic freshwater basal media
152 (ATCC 51573) at 32 °C (Lovely and Phillips, 1988). Cells for all experiments were grown by
153 first inoculating an anaerobic serum bottle containing 50 mL of freshwater basal media, and
154 incubating it for 5 days at 32 °C. Cells were pelleted by centrifugation at 8100g for 5 minutes,
155 and rinsed 5 times with 0.1 M NaClO₄ stripped of dissolved oxygen by bubbling a 85%/5%/10%
156 N₂/H₂/CO₂ gas mixture through it for 30 minutes. After washing, the three types of bacteria used
157 in this study were then pelleted by centrifugation at 8100g for 60 minutes to remove excess water
158 to determine the wet mass so that suspensions of known bacterial concentration could be created.

159 Experimental conditions for all the cell cultures described above represent the early
160 exponential phase of the bacterial growth curves.

161 *2.2 Hg Adsorption Experiments*

162 A 200 ppm parent solution of Hg²⁺ in 0.1 M NaClO₄ was prepared from a commercially-
163 supplied 1000 ppm Hg in nitric acid reference solution, which was adjusted to pH 3.0 by adding
164 aliquots of 1 M NaOH. Appropriate amounts of the Hg(II) parent solution were added to achieve
165 the desired Hg(II) and bacterial concentrations (Table S1). The concentration of the bacterial
166 suspensions was 2 g L⁻¹ (~ 10¹³ cell L⁻¹) for all of the experiments in this study. The pH of each
167 system was adjusted to 5.5 (± 0.2) using small aliquots of 1 M HNO₃ or NaOH, and the systems
168 were allowed to react for two hours on a shaker at room temperature (22 °C). Since surface
169 waters exposed to the atmosphere have a pH of approximately 5.6 due to the dissolution of
170 carbon dioxide into the water, we chose to work at pH 5.5 to make our results relevant to
171 environmental and geochemical systems. Metal adsorption on bacterial cell surfaces have been
172 previously conducted at similar pH conditions (Boyanov et al., 2003; Claessens and Van
173 Cappellen, 2007; Wei et al., 2011). In addition, we conducted experiments at pH 5.5 to exclude
174 potential effects of insoluble Hg-hydroxide formation which are highly favorable at alkaline pH
175 conditions. pH was monitored every 30 min, and adjusted as required. After 2 h of reaction, the
176 suspensions were centrifuged, and the bacterial pellet from each experiment was retained for
177 XAFS analysis. The supernatant was filtered (0.45 µm) using nylon membranes (Millipore
178 filter), acidified, and analyzed for dissolved Hg(II) by inductively coupled plasma-optical
179 emission spectroscopy (ICP-OES; Perkin-Elmer). Filtering supernatant using Fluoropore PTFE
180 membranes filter (0.45 µm) did not result in appreciable change in the concentration of Hg in
181 supernatant.

182
183 Previous experiments (Fowle and Fein, 2000) have demonstrated the reversibility of
184 metal binding reactions under similar experimental conditions, strongly suggesting that the
185 metals are not internalized during the course of the experiments.

187 *2.3 Hg XAS Measurements and Data Analysis*

188 Hg L_{III} edge X-ray absorption near edge structure (XANES) and extended X-ray
189 absorption fine-structure spectroscopy (EXAFS) measurements were performed at the MRCAT
190 sector 10-ID beamline (Segre et al., 2000), Advanced Photon Source, at Argonne National
191 Laboratory. The continuous scanning mode of the undulator was used with a step size and
192 integration time of 0.5 eV and 0.1 s per point, respectively, in order to decrease the radiation
193 exposure during a single scan. In addition, the measurements were conducted at different spots
194 on the sample to further decrease the time of exposure. XANES spectroscopy, which is sensitive

195 to chemical changes in the sample, was constantly monitored for any possible radiation damage.
196 Successive XANES scans did not show any beam induced changes in any of the samples studied
197 (data not shown).

198
199 Hg XANES and EXAFS measurements and the data analysis approach for this study
200 were similar to those previously published by our group (Mishra et al., 2011; Pasakarnis et al.,
201 2013; Dunham-Cheatham et al., 2014; Dunham-Cheatham et al., 2015). The data were analyzed
202 using the methods described in the UWXAFS package (Stern et al., 1995). Energy calibration
203 between different scans was maintained by measuring a Hg/Sn amalgam, prepared as described
204 elsewhere (Harris et al., 2003), on the reference chamber concurrently with the fluorescence
205 measurements of the biomass-bound Hg samples. The inflection point of the Hg L_{III} edge
206 (12.284 KeV) was used for calibration of the scans. Data processing and fitting was done with
207 the programs ATHENA and ARTEMIS (Ravel and Newville, 2005). The data range used for
208 Fourier transforming the k space data was 2.3–9.8 Å⁻¹, except in the case of the two lowest Hg
209 concentration samples where 2.3–8.2 Å⁻¹ was used due to poor data quality. The Hanning
210 window function was used with a dk of 1.0 Å⁻¹. Fitting of each spectrum was performed in r -
211 space, from 1.2–3.2 Å, with multiple k -weighting (k^1 , k^2 , k^3) unless otherwise stated. Lower χ^2
212 (reduced chi square) was used as the criterion for inclusion of an additional shell in the shell-by-
213 shell EXAFS fitting procedure.

214 215 2.4 Hg XAS Standards

216 Crystalline powder standards (cinnabar [red HgS] and mercuric acetate) were measured
217 and used to calibrate the theoretical calculations against experimental data. Data from the
218 standards were analyzed to obtain the $S0^2$ parameter, where $S0^2$ is the value of the passive
219 electron reduction factor used to account for the many body effects in EXAFS. By fixing the
220 value of S and O atoms to 2 in cinnabar and mercuric acetate, we obtained $S0^2$ values of $1.02 \pm$
221 0.05 and 0.98 ± 0.03 , respectively. Hence, we chose to set the value of $S0^2$ to be 1.0 for all the
222 samples. Fitting of the powder standards to their known crystallographic structure (cinnabar and
223 mercuric acetate) reproduced the spectral features in the entire fitting range (1.0–4.2 Å) and the
224 fitting parameters were in agreement with previously reported values (Almann, R., 1973;
225 Manceau and Nagy, 2008). Only the paths necessary to model the solid standards were used for
226 fitting the solution standards and the unknown Hg samples.

227 In addition to crystalline powder standards, solution-phase standards (Hg²⁺, Hg-cysteine,
228 and Hg-acetate) were also measured as solution standards in order to provide a better
229 representation of aqueous metal speciation than crystalline powder standards. Aqueous Hg²⁺ and
230 Hg-cysteine standards were prepared from high purity 5mM Hg²⁺ in 5% HNO₃ bought from GFS
231 Chemicals. Hydrated Hg²⁺ was adjusted to pH 2.0 for measurement by adding appropriate
232 amounts of 5 M NaOH. A Hg-cysteine standard was prepared by adding cysteine to 5mM Hg²⁺
233 in 5% HNO₃ in a Hg:ligand ratio of 1:100. The pH of the Hg-cysteine solution was adjusted to
234 5.0 and 8.0 by adding appropriate amounts of 5 or 1 M NaOH to obtain solutions with
235 predominantly Hg-(cysteine)₂ and Hg-(cysteine)₃ present, respectively. It must be emphasized
236 that solution species are almost always a mixture of different Hg-cysteine species. Although the
237 presence of small fractions (less than 10%) of other stoichiometries of Hg-cysteine complexes in
238 the Hg-(cysteine)₂ and Hg-(cysteine)₃ standards cannot be ruled out, comparison of the Hg-S
239 bond lengths determined using EXAFS modeling of these standards with published values was
240 used to validate their stoichiometries. The Hg-acetate standard was prepared by adding mercuric-

241 acetate salt to ultrapure water and the pH of this solution was adjusted to 5.0 by adding
242 appropriate amounts of 1 and 5 M NaOH. The best fit values of the Hg-(cysteine)₂, Hg-
243 (cysteine)₃, and Hg-acetate solution standards were used as the initial values of the
244 corresponding variables for fitting the unknown Hg biomass samples.

245

246 *2.5 S XANES Measurement and Analysis*

247 Sulfur K-edge XANES spectra for biomass samples were acquired at the National
248 Synchrotron Light Source (NSLS, Brookhaven) on beamline X19A using a PIPS detector in
249 fluorescence detection mode. At X19A, signal from higher order harmonics was removed by
250 detuning the monochromator to 70% of the maximum beam flux at 2472.0 eV. An energy
251 calibration was performed by setting the first peak in the spectrum of sodium thiosulfate salt
252 (Na₂S₂O₃), corresponding to the thiol S, to 2469.2 eV. XANES spectra were typically measured
253 between 2450 and 2500 eV. Step sizes in the near-edge region (2467-2482 eV) were 0.08 eV,
254 and 0.2 eV in pre- and post- edge regions.

255

256 *2.6 Thiol Quantification with qBBr Titrations*

257 The concentration of bacterial cell envelope thiols was quantified by reacting a known
258 cell density with increasing concentrations of qBBr in water and detecting fluorescence with a
259 Photon Technology International Quantamaster fluorometer. The qBBr was purchased from
260 Sigma-Aldrich and Toronto Research Chemicals. When excited at 380 nm, the qBBr-thiol
261 complex has a maximum emission at 470 nm. When emission intensity is plotted against qBBr
262 concentration, the thiol concentration in the cell suspension is evident by a decrease in the slope
263 of intensity per qBBr concentration to the background level (the fluorescence of qBBr in water).
264 Optical density of the cells in water at 260 nm was below the detection limit of the
265 spectrophotometer, indicating low DNA concentrations which could result from cell lysis.
266 Further details about this method are provided elsewhere (Joe-Wong et al., 2012).

267

268 *2.7 Thiol Determination with Potentiometric Titrations*

269 The change in total site concentrations on cell envelopes determined by potentiometric
270 titrations of biomass with and without qBBr treatment was used as a direct measure of the thiol
271 site concentration. Details of the procedure and modeling approach are given in Yu et al. (2014).
272 Briefly, bacterial suspensions were allowed to react for 2 h with a qBBr-bearing solution with a
273 qBBr:bacteria ratio of 130 μmol qBBr/g (wet biomass), followed by three rinses. Potentiometric
274 titrations in de-gassed 0.1 M NaCl were conducted under a headspace of N₂ gas to exclude
275 atmospheric CO₂ and each suspension was stirred continuously.

276 **3.0 Results**

277 *3.1 Hg adsorption*

278 Hg adsorption on the three bacterial species over four orders of magnitude is shown in
279 table S1. Hg was found to be below the detection limit of ICP under low aqueous Hg
280 concentration regime suggesting that Hg adsorbs strongly onto bacterial cells, with nearly
281 complete removal of Hg from aqueous solutions under these experimental conditions. Increase in
282 aqueous Hg concentration resulted in lower fraction of adsorbed Hg for all the three species
283 examined. These trends demonstrate that the total number of deprotonated sites around pH 5.5
284 are similar for all the three species. Previous study has shown the transition from reduction of Hg

285 to adsorption of Hg associated with biomass concentrations of 10^{10} to 10^{13} cells/L (Hu et al.,
286 2013). Since the experiments presented here contain 10^{13} cells/L, we rule out reduction of Hg in
287 our study. It should also be noted that a rigorous Hg mass balance has not been presented here.
288 Mass balance is not relevant for this study and does not affect any of our results or conclusions
289 because our work focuses on elucidating the mechanism of complexation of Hg with cell
290 membranes.

291

292 3.2 Qualitative XAS Analysis of Hg Standards

293 The XANES spectra for the solution-phase Hg^{II} standards (Hg²⁺, Hg-acetate, Hg-
294 (cysteine)₂, and Hg-(cysteine)₃) are shown in Figure 1. The XANES spectra of these three
295 standards have significantly different spectral features (Figure 1): Hg²⁺ is out of phase with the
296 rest of the standards presented here and has a distinct peak at 12310 eV; Hg-acetate has a
297 pronounced pre-edge feature at about 12285 eV; the Hg-(cysteine)₂ complex exhibits a much
298 smaller pre-edge feature at 12290 eV than the Hg-acetate complex and exhibits another shoulder
299 at 12300 eV; the Hg-(cysteine)₃ has a further smaller pre-edge peak (with 12290 and 12300 eV
300 shoulder missing) and has a distinctly different post-edge shape which is easily distinguishable
301 from the Hg-(cysteine)₂ standard and the rest of the standards presented here. Comparison of the
302 XANES spectra for the Hg-(cysteine)₂ and Hg-(cysteine)₃ standards can be seen in Figure S1a.

303

304 A shift to higher radial distance in the first peak of the Fourier transformed (FT) data for
305 the Hg-(cysteine)₂ spectrum relative to the Hg-acetate standard spectrum, arising from the
306 bonding of Hg to sulfur in the first shell as opposed to bonding to oxygen, can be seen in Figure
307 2. The longer distance of the first peak for the Hg-(cysteine)₂ spectrum compared with the Hg-
308 acetate standard is concomitant with a larger amplitude of the FT EXAFS data for the Hg-
309 (cysteine)₂ as expected from a heavier backscatterer (Figure 2). In addition, the radial distance for
310 the first peak of the Hg-(cysteine)₃ standard is longer than that of the Hg-(cysteine)₂ standard,
311 also evident in the phase shift of the Hg-(cysteine)₃ standard towards lower k value (Figure S1).
312 However, the Hg-(cysteine)₃ standard has a smaller amplitude than the Hg-(cysteine)₂ standard
313 because a distorted trigonal planer structure has a larger structural disorder associated with it
314 compared to the linear Hg-(cysteine)₂ complex. Hence, careful comparison of the XANES and
315 EXAFS data from the Hg biomass samples can be used to determine whether the Hg associated
316 with biomass is bound to the biomass through Hg –carboxyl or –thiols, and the stoichiometry of
317 Hg:thiol complexes can also be determined from the data.

318

319 3.3 Quantitative XAS Analysis of Hg Standards

320 Best fit values resulting from EXAFS analysis of the solution standards are given in
321 Table 1. The aqueous Hg²⁺ standard was best fit with Hg being bound to 6.12 (\pm 0.65) O atoms
322 at 2.30 (\pm 0.01) Å, which is consistent with an octahedral coordination geometry of a hydrated
323 Hg²⁺ ion (Richens, D. T., 1997). Hg-acetate was best fit with 1.78 (\pm 0.32) O atoms at 2.06 (\pm
324 0.01) Å in the first shell. The number of C atoms, which was fixed to be equal to the number of
325 O atoms in the first shell, was found at 2.83 (\pm 0.01) Å, consistent with the crystal structure of
326 mercuric acetate (Almann, R., 1973). The Hg-(cysteine)₂ solution was best fit with 1.88 (\pm 0.21)
327 S atoms at 2.32 (\pm 0.01) Å in the first shell, which indicates complexation of Hg with two
328 cysteine moieties (Manceau and Nagy, 2008). Inclusion of C atoms did not lower the χ^2 (Stern
329 et al., 1995) value significantly enough to justify the addition of another shell. The Hg-
330 (cysteine)₃ solution was best fit with 2.82 (\pm 0.32) S atoms at 2.49 (\pm 0.01) Å in the first shell.

331 Published literature suggests that a Hg-S bond distance of 2.49 Å is representative of the Hg-S₃
332 complex, but could possibly include small components of Hg-S₂ and Hg-S₄ complexes as well
333 (Manceau and Nagy, 2008; Warner and Jalilehvand, 2016). In summary, the fitting parameters
334 for the solution standards reported in this study are in good agreement with previously published
335 values (Xia et al., 1999; Qian et al., 2002; Skyllberg et al., 2006; Mishra et al., 2011; Thomas et
336 al., 2016).

337 3.4 Hg(II) complexation with biomass

338 The following conclusions can be drawn concerning Hg binding onto the biomass
339 samples, and the descriptions in this section describe the evidence for these conclusions in more
340 detail. Hg(II) was found to complex entirely with thiols at low Hg:biomass ratios. The Hg
341 coordination changed from Hg-S₃ to Hg-S₂ and Hg-S progressively as the Hg(II) loading
342 increased on the cells. These Hg-S_n (where n=1-3) bacterial surface complexes also exhibit
343 different Hg-S bond distances (2.3-2.5 Å) with the longest in the Hg-S₃ complex, consistent with
344 published literature (Manceau and Nagy, 2008). Upon saturation of the high affinity thiol sites at
345 higher Hg:biomass ratios, Hg²⁺ was found to form a chelate with carboxyl and a neighboring
346 hydroxyl (α -hydroxy carboxylate anion) based on the measured Hg-O and Hg-C distances (Table
347 1). Such α -hydroxy carboxylic acids have been reported to occur abundantly within cell
348 envelopes (Wei et al., 2004). While all the species exhibit strong affinities for Hg²⁺ at low
349 Hg:biomass ratios, the differences in Hg-S stoichiometry between the cell envelopes of *S.*
350 *oneidensis* MR-1 and *G. sulfurreducens* is noteworthy.

351 3.4.1 Hg(II) complexation with *Shewanella oneidensis* MR-1

352 Figure 1a shows the XANES data of Hg(II) complexed to *Shewanella oneidensis* MR-1
353 biomass as a function of Hg loading. Comparison of the XANES spectra for the Hg-biomass
354 samples with the Hg standards suggests that the transition from thiol to carboxyl functional
355 groups takes place around 50 μ M Hg(II). A systematic change in the amplitude and phase shift of
356 oscillations in the k^2 -weighted $\chi(k)$ data of the Hg-biomass samples can be seen in Figure 2a. Hg
357 is complexed exclusively via thiols in samples containing less than 50 μ M Hg(II), while Hg is
358 complexed exclusively via carboxyl functional groups in samples containing more than 50 μ M
359 Hg(II). Samples containing 0.5 μ M or less Hg(II) have a spectral signature of Hg-(cysteine)₃
360 binding. The FT EXAFS data from the biomass samples with 350, 15, and 0.5 μ M Hg(II) have
361 spectral features and first shell bond distances similar to the following aqueous Hg standards
362 respectively: Hg-acetate, Hg-(cysteine)₂, and Hg-(cysteine)₃ (Figure 3a). The differences
363 between the amplitude and bond distances of the 350, 15, and 0.5 μ M Hg(II) samples and their
364 similarities with Hg-acetate, Hg-(cysteine)₂, and Hg-(cysteine)₃ solution standards, respectively,
365 are further illustrated in the real part of the Fourier transforms shown in Figure 3b. Based on
366 bond distances and amplitude of the FT data, the Hg-biomass samples can be divided into three
367 sub-groups: 350-50 μ M Hg(II), 25-5 μ M Hg(II), and 0.5 μ M Hg(II) (Figures 1 and 3). These
368 three sub-groups of biomass samples appears to be dominated by Hg-carboxyl, Hg-(cysteine)₂,
369 and Hg-(cysteine)₃ binding environments, respectively. The 2.5 μ M Hg(II) sample can be well-
370 described by a linear combination of the 0.5 and 5.0 μ M Hg(II) biomass samples, suggesting that
371 Hg-(cysteine)₂ and Hg-(cysteine)₃ coordination environments comprise approximately 58 and
372 42% (\pm 5%) of the bound Hg, respectively.
373

374 The Hg-biomass data were modelled quantitatively as described above. Best fit values are
375 given in Table 1. The 350 μM Hg(II) data was best fit with 1.65 (± 0.25) O atoms at 2.06 (\pm
376 0.01) \AA in the first shell. Inclusion of 1.58 (± 0.32) C atoms in the second shell resulted in
377 significant improvement of the fit. However, the Hg-C distance for this sample was 3.05 (± 0.02)
378 \AA , which is much longer than the Hg-C distance determined for the Hg-acetate solution standard
379 (2.83 ± 0.01 \AA). This suggests the formation of a carboxyl with alpha-hydroxy carboxylic acid or
380 a malate type coordination geometry for the biomass samples. The 100 and 50 μM Hg(II) data
381 did not show any appreciable change in the coordination environment, except that the 50 μM
382 Hg(II) data was improved by inclusion of S atoms in the first shell. The coordination number of
383 S was 0.56 (± 0.12), suggesting a small fraction of Hg atoms bound to thiols for this sample. The
384 25 μM Hg(II) biomass sample was best fit with 1.32 (± 0.21) S atoms at about 2.31 (± 0.01) \AA in
385 the first shell. The 15 and 5 μM Hg(II) samples were best fit with ~ 1.8 (± 0.2) S atoms at about
386 2.32 (± 0.02) \AA in the first shell. The 2.5 μM Hg(II) sample was best fit as a linear combination
387 of Hg-(cysteine)₂ and Hg-(cysteine)₃ coordination environments, with ~ 2.2 (± 0.3) S atoms at
388 about 2.44 (± 0.01) \AA in the first shell. The 0.5 μM Hg(II) sample was mostly Hg-(cysteine)₃
389 with 2.96 (± 0.25) S atoms at 2.51 (± 0.01) \AA . Inclusion of an O/N atom in the first shell or a C
390 atom in the second shell did not result improve the fit for the samples containing 25 μM Hg(II)
391 or less.

392
393 A recent study has suggested the formation of a Hg-S₄ complex on *E. coli* cells under
394 actively metabolizing conditions (Thomas et al., 2016). While the experimental conditions
395 studied by Thomas et al. (2016) are different from those in this study, formation of Hg-S₄
396 complex on bacterial cells is unlikely at circumneutral pH conditions because Hg-(cysteine)₄
397 solution complexes are formed only under highly alkaline conditions (Warner and Jalilehvand,
398 2016). Thomas et al. (2016) also conducted XAS measurements at very low temperatures, which
399 can induce the formation of tetrathiolate complexes (Nagy et al., 2011). Further, biochemical
400 considerations support the existence of Hg-(cysteine)₃ but not Hg-(cysteine)₄ complexes on cell
401 envelopes (Cheesman et al., 1988).

402
403 Although it is possible that Hg goes on to N (amines) sites after saturating S (thiols) sites
404 which constitute a small number of sites and quickly get masked by transition of Hg to O
405 (carboxyl) sites which are much more abundant, we do not see any evidence for the same. Hg
406 XANES for Hg-histidine aqueous solution does not resemble Hg-biomass samples at high Hg
407 loadings (figure S2).

408 409 3.4.2 Hg(II) complexation with *Bacillus subtilis* and *Geobacter sulfurreducens*

410 A similar approach was adopted to model the Hg-biomass data for the *B. subtilis* and *G.*
411 *sulfurreducens* samples. Trends similar to the *S. oneidensis* MR-1 data can be seen in the k^2 -
412 weighted $\chi(k)$ EXAFS data of the Hg biomass samples for *B. subtilis* and *G. sulfurreducens*
413 (Figure 3). Figures S3a and S3b show the XANES and figures S4a and S4b show the data and fit
414 of the EXAFS FT magnitude for *B. subtilis* and *G. sulfurreducens* samples, and the best fit
415 values for the Hg EXAFS modeling are provided in Table 1.

416 In the case of *B. subtilis*, the 350, 100, and 75 μM Hg(II) samples were modeled
417 exclusively as Hg-carboxyl binding, and did not exhibit any signature of thiol complexation of
418 Hg. The 25 and 15 μM samples for *B. subtilis* were found to have some Hg-thiol complexation

419 with a larger fraction of the Hg atoms complexed with carboxyl groups, similar to the 50 μM
420 Hg(II) sample for *S. oneidensis* MR-1. The *B. subtilis* samples with 5.0, 2.5, and 0.5 μM Hg(II)
421 were modeled with 1.80 ± 0.2 , 1.95 ± 0.3 , and 2.26 ± 0.3 S atoms at 2.32 ± 0.01 , 2.33 ± 0.01 , and
422 2.45 ± 0.01 respectively. The 5.0 and 2.5 μM Hg(II) samples exhibit Hg-(cysteine)₂ coordination
423 environment. The 0.5 μM Hg sample for *B. subtilis* is a combination of Hg-(cysteine)₂ and Hg-
424 (cysteine)₃ coordination environments, similar to the 2.5 μM Hg sample for *S. oneidensis* MR-1.
425 In summary, the stoichiometry of Hg(II) on Gram-positive *B. subtilis* cells follows the same
426 trend as we observed for the Gram negative *S. oneidensis* MR-1 cells. However, the transition
427 from carboxyl to thiol and Hg-(cysteine)₂ to Hg-(cysteine)₃ complexation takes place at lower
428 Hg(II) concentrations for the *B. subtilis* samples. Differences in the abundance of thiols within
429 the cell envelopes of *B. subtilis* and *S. oneidensis* MR-1 (see below) are likely to explain the
430 offset in Hg(II) concentration between these two species at which the transition in binding
431 environment occurs.

432 The Hg EXAFS analysis of the 75 μM Hg sample for *G. sulfurreducens* indicated that a
433 small fraction of Hg was bound to thiol sites, with a majority of the Hg bound to carboxyl, which
434 was similar to what we observed for the 50 and 25 μM Hg samples for *S. oneidensis* MR-1 and
435 for *B. subtilis*, respectively. This observation suggests an offset in the loading of Hg(II) at which
436 Hg binding transitions from predominantly carboxyl to thiol for *G. sulfurreducens* compared
437 with *S. oneidensis* MR-1 and *B. subtilis*. However, the offset in Hg(II) loading in the case of *G.*
438 *sulfurreducens* is opposite to that of *B. subtilis*. Since the signature of Hg-(cysteine)₃ binding was
439 observed for the *B. subtilis* samples at lower Hg(II) concentration than for the *S. oneidensis* MR-
440 1 samples, it would be expected that the stoichiometry of Hg(II) complexation with *G.*
441 *sulfurreducens* cells would transition from Hg-(cysteine)₂ to Hg-(cysteine)₃ at higher Hg(II)
442 concentrations than was observed for *S. oneidensis* MR-1. Nevertheless, Hg-S bond distances
443 and coordination numbers for *G. sulfurreducens* changed only slightly from 2.32 ± 0.01 Å and
444 1.70 ± 0.2 for the 25 μM Hg sample to 2.38 ± 0.01 Å and 2.24 ± 0.2 for the 0.5 μM Hg sample,
445 suggesting a lack of formation of Hg-(cysteine)₃ stoichiometry within the *G. sulfurreducens* cell
446 envelope (Figures 2c and 2d). This result is somewhat surprising, and could provide important
447 clues about Hg bioavailability for intracellular biochemical process (more below).
448

449 3.5 Sulfur XANES

450 Although the S K-edge XANES spectra were collected on a large number of standards, in
451 this study we have broken down the S species into three main categories for the sake of clarity:
452 reduced S (below 2472 eV), sulfoxide S (near 2473.5 eV), and oxidized S (above 2476.5 eV).
453 Cysteine, dimethyl sulfoxide (DMSO), sodium dodecylsulfate (NaDS), and sodium laurel sulfate
454 Na₂SO₄ standards are shown in Figure 4a. More extensive model libraries that include XANES
455 spectra of organic and inorganic S compounds are available in the literature (Vairavamurthy A.,
456 1998; Myneni, S. C. B., 2002). As seen in Figure 4a, species with very different S oxidation
457 states such as cysteine, sulfoxide, and ester sulfate are easily resolved in the XANES spectrum.
458 Within these three energy ranges, however, resolution becomes more difficult. Reduced sulfur
459 species, including thiols, sulfides, polysulfides, and thiophenes, all have white-line features
460 occurring between 2469 and 2472 eV. S K-edge XANES shows sensitivity to changes in the
461 electronic environment of the sulfur absorber. For example, perturbation in the electron donating
462 ability of the organic moiety changes the energy positions of pre-edge features by affecting the
463 effective nuclear charge on the sulfur atom (Szilagy and Schwab, 2005).

464 The S-XANES spectrum of the *S. oneidensis* MR-1 cells cultured under different
465 conditions (aerobic, nitrate, fumarate) and titrated to pH values ranging from pH 4 to 8, indicate
466 a high abundance of reduced S groups (e.g. mono-, and disulfide) relative to the oxidized forms
467 of S (e.g., sulfate, sulfonate) (Figure 4b and 4c). However, monosulfides, such as S in
468 methionine and cysteine, exhibit similar spectral features and are hard to distinguish
469 (Vairavamurthy, A., 1998; Xia et al., 1998; Myneni, S. C. B., 2002; Szilagy and Schwab, 2005;
470 Risberg et al., 2009). Because thiols are known to exhibit stronger interactions with Hg(II)
471 among these reduced monosulfides (or thioether), we conclude that Hg(II) must be interacting
472 with thiols and our Hg-thiol stoichiometry results obtained using Hg XAS are likely independent
473 of experimental pH (except in extreme environments) and cell culturing conditions.

474 Interaction of Hg(II) with thiols within cell envelopes is also evident from the changes in
475 S XANES spectra as a function of Hg(II) loading. When the bacterial cells were exposed to
476 increasing levels of Hg(II), the pre-edge feature of the S XANES spectra of the cell suspensions
477 indicated gradual changes in S-speciation, corresponding to the deprotonation and subsequent
478 complexation of thiol with Hg²⁺ (Figure S5; Risberg et al., 2009; Szilagy and Schwab, 2005).
479 The pre-edge feature of the S K-edge XANES data (figure S5) as a function of Hg loading on *S.*
480 *oneidensis* MR-1 suggests the deprotonation of cysteine at higher Hg loadings (Szilagy and
481 Schwab, 2005).

482 3.6 Thiol Quantification with qBBR Titrations

483 qBBR is a large, thiol-sensitive, charged, water-soluble fluorophore molecule, which does
484 not cross the cell envelope, making it an ideal probe for measuring the concentration of thiols
485 within the cell envelope (Joe-Wong et al., 2012; Rao et al., 2014). Our qBBR titrations suggest
486 that the concentration of reactive thiols within the cell envelopes of *B. subtilis*, *S. oneidensis*
487 MR-1, and *G. sulfurreducens* are 24±2, 49±12, and 240±80 μM/g wet weight cells, respectively.
488 These wet weight values correspond to 120±10, 300±70, and 1000±300 μM/g dry weight cells,
489 respectively (Figure 5a; Table 2). The cell envelope thiol concentrations determined using qBBR
490 fluorophore measurements for *B. subtilis* and *S. oneidensis* MR-1 are in good agreement with
491 published results (Joe-Wong et al., 2012). These results are also in excellent agreement with the
492 Hg EXAFS analyses (described above) showing the transition of Hg speciation from Hg-
493 carboxyl binding to Hg-thiol complexation for *B. subtilis* and *S. oneidensis* MR-1 at
494 approximately 25 and 50 μM Hg(II), respectively. However, thiol concentrations for *G.*
495 *sulfurreducens* obtained from the qBBR measurements in this study are higher than those recently
496 reported by another study using a similar technique (Rao et al., 2014) and our Hg EXAFS
497 analyses. If thiol concentrations on *G. sulfurreducens* were as small as previously reported (Rao
498 et al., 2014), Hg complexation with thiols would saturate all the thiol sites on *G. sulfurreducens*
499 cells at much lower Hg(II) concentrations, and transition from Hg-thiol coordination
500 environment to Hg-carboxyl interactions at much lower Hg(II) loading. Hence, our Hg EXAFS
501 results do not agree with the thiol quantification on *G. sulfurreducens* either from this study or
502 with those reported previously (Hu et al., 2013; Rao et al., 2014). To resolve these differences
503 another direct measurement of the thiol site concentrations on *G. sulfurreducens* cells was
504 conducted using potentiometric titrations with and without qBBR treatment of *G. sulfurreducens*
505 cells.

506 3.7 Thiol Determination with Potentiometric Titrations

507 Potentiometric titrations (see Yu et al., 2014 for details) were performed on *G.*
508 *sulfurreducens* with and without qBBr treatment to resolve the difference of over two orders of
509 magnitude between the qBBr measurements reported in this study and those reported previously.
510 Potentiometric titration measurement on *G. sulfurreducens* cells resulted in a calculated thiol
511 concentration of $67.8 \pm 22.8 \mu\text{mol/gm}$ wet weight (Figure 5b; Table 3). This value is in good
512 agreement with our Hg EXAFS estimation of $\sim 75 \mu\text{M}$ thiol sites/g wet weight cells, which is an
513 indirect measurement of the abundance of thiols within the *G. sulfurreducens* cell envelope
514 (Table 1).

515 4.0 Discussion

516 Complexation of Hg with high affinity thiol sites under low metal loading conditions,
517 followed by binding of Hg to lower affinity carboxyl sites upon saturation of thiol sites has been
518 documented previously (Mishra et al., 2011). Similar behavior has also been observed for Zn and
519 Cd (Guiné et al. 2006; Mishra et al., 2010; Yu and Fein, 2015). Association of Hg with reduced
520 S groups has also been shown in phytoplankton (diatoms) collected from a Hg contaminated
521 creek using a combination of x-ray micro-fluorescence mapping and FTIR studies (Gu et al.,
522 2014).

523 This study demonstrates that Hg complexation with intact bacterial cell suspensions, a
524 mechanism which is likely applicable to other chalcophilic metals (e.g. Zn, Cd, and Pb) as well,
525 is strongly dependent on metal loading and that the following conclusions can be drawn: 1)
526 complexation of Hg with cell bound thiols is much more complicated than the formation of a
527 single type of Hg-thiol complex at low Hg:biomass ratios; and 2) Hg can be complexed with
528 cell-bound thiol sites in a variety of stoichiometries depending on the biogeochemical attributes
529 of the ecosystem in question (e.g., the Hg:biomass ratio, the abundance of thiol sites on the
530 bacterial species in question, and whether the species is Hg-methylating or not). It must be
531 emphasized that in contrast with expectation from purely thermodynamic considerations,
532 variation in the complexation behavior of Hg with thiols is not always dictated by the abundance
533 of thiols on a given bacterial species.

534 Our results illustrate that *B. subtilis* and *S. oneidensis* MR-1 cells show similar Hg
535 complexation behavior with cell bound thiols, albeit, the transition from Hg-S₂ to Hg-S₃ occurs
536 at lower Hg loadings for *B. subtilis* due to lower thiol abundance compared to *S. oneidensis* MR-
537 1. Although lower thiol concentrations in the case of *B. subtilis* prevented detailed examination
538 of Hg-thiol interactions using Hg EXAFS below $0.5 \mu\text{M}$ Hg(II), as expected, *B. subtilis* formed
539 Hg-S₂ and Hg-S₃ complexes at a lower Hg:biomass ratio than *S. oneidensis* MR-1.

540 While *B. subtilis* and *S. oneidensis* MR-1 exhibit the general trend outlined above,
541 significant differences in Hg-thiol interactions were found between *G. sulfurreducens* and *S.*
542 *oneidensis* MR-1 at low Hg(II) concentrations. In the case of *S. oneidensis* MR-1, Hg forms the
543 Hg-S₃ complex below aqueous Hg concentrations of $0.5 \mu\text{M}$, but forms Hg-S₂ and Hg-S
544 complexes at higher Hg concentrations (Table 1). In contrast, under the same Hg concentration
545 conditions, the Hg methylating species *G. sulfurreducens* forms only Hg-S₂ and Hg-S complexes
546 without a detectable Hg-S₃ complex. This difference in surface complexation of Hg on the *G.*
547 *sulfurreducens* cells was not caused by the lack of sufficient thiols on *G. sulfurreducens*. As
548 shown above, *G. sulfurreducens* has the highest abundance of thiols among the three species
549 examined. Although a definitive reason for the inconsistent behavior of *G. sulfurreducens* cell

550 envelope compared to those of *S. oneidensis* MR-1 and *B. subtilis* is beyond the scope of this
551 study, these differences could provide insights about Hg cell surface complexes for methylating
552 vs. non-methylating species. We hypothesize that the differences in the membrane protein
553 chemistry (Hg transporters) and Hg uptake mechanism of *G. sulfurreducens* inhibits *G.*
554 *sulfurreducens* to form Hg-S₃ type complexes unlike other two species examined. Our
555 hypothesis is strengthened by a previous study which shows that aqueous Hg-S₂ complexes
556 enhances Hg(II) uptake and subsequent methylation by *G. sulfurreducens* while aqueous Hg-S₃
557 complexes inhibit the same (Schaefer and Morel, 2009). In order to form Hg-S₃ complexes
558 within cell envelopes, cell surface proteins must contain at least 3 thiol sites in close proximity to
559 each other. Although *G. sulfurreducens* exhibits the highest concentration of thiols among the
560 examined bacterial species, the thiol site density (i.e. sites/A²) of *G. sulfurreducens* must not be
561 high enough to make tridentate Hg-S₃ complex. These results suggest that the cell envelope S-
562 amino acid containing proteins are significantly different between *G. sulfurreducens* and *S.*
563 *oneidensis* MR-1, specifically their density and reactivity, which are critical in Hg binding,
564 transport and possibly uptake. However, these results could be specific to a given bacterial
565 species. Hence our results should not be generalized in the broader context of Hg-methylators vs.
566 non-methylators without additional studies.

567 Differences in abundance and density of thiol sites on cells of different bacterial species,
568 and the corresponding stoichiometry of Hg-thiol complexes that arise from those differences,
569 could also explain the observed differences in passive oxidation of Hg(0) mediated by cell bound
570 thiols (Colombo et al., 2014). These cell envelope bound Hg-S_n complexes also form readily in
571 the presence of other strongly competing ligands, such as Cl⁻ and NOM (which also contains
572 thiols), and were found to be stable in aqueous solutions at room temperature for over a period of
573 2 months (Figure S6; Dunham-Cheatham et al., 2014; Dunham-Cheatham et al., 2015). While
574 the cell envelope-bound Hg-thiol complexes constitute the pool of Hg(II) transported inside the
575 cell for Hg-methylation in the case of *G. sulfurreducens*, Hg-S₃ complexes in the non-
576 methylating bacterial species *B. subtilis* and *S. oneidensis* MR-1 would likely stay as Hg-S_n
577 complexes until the amino acid residue is oxidized. Given the high thermodynamic stability of
578 Hg-S₃ complexes, they are not expected to be released back into the aqueous phase as thiol
579 complexes. Alternatively, they could slowly transform into inorganic Hg-sulfide (e.g. meta-
580 cinnabar) nanoparticles under sulfidic environments. It has been recently shown that Hg forms
581 colloidal meta-cinnabar when reacted with DOM in the presence of sulfide, presumably via
582 reaction with thiols in the DOM (Gerbig et al., 2011). It remains to be determined if thiols
583 present within bacterial cell envelopes could also mediate the formation of meta-cinnabar,
584 limiting the bioavailability of Hg for microbial processes (Zhang et al., 2012). Since bacteria are
585 ubiquitous in all natural systems, and their cell envelope-bound reactive thiol site concentrations
586 often exceed the aqueous concentrations of Hg in many natural and contaminated settings, this
587 study suggests that cell envelope-bound thiol sites play a key role in the speciation, fate and
588 bioavailability of Hg in aquatic and terrestrial ecosystems.

589

590

591

592

593 **ACKNOWLEDGMENTS**

594 The authors would like to dedicate this paper to the memory of Prof. Terry Beveridge,
595 with whom collaborations began many years ago to investigate bacterial cell envelopes. The
596 authors are grateful to Tamar Barkay and Francois Morel for their thoughtful discussions and
597 comments. This work was funded by DOE-Subsurface Biogeochemical Research (SBR), and
598 NSF (Chemical and Earth Sciences). BM was partially supported by the Argonne Subsurface
599 Scientific Focus Area (SFA) project during the preparation of this manuscript, which is part of
600 the SBR Program of the Office of Biological and Environmental Research (BER), U.S. DOE
601 under contract DE-AC02-06CH11357. We are thankful to Jennifer Szymanowski and Madhavi
602 Parikh for help with sample preparation, Dr(s). Tomohiro Shibata and Sayed Khalid for their
603 help in beam line set-up and XAS measurements, and Dr. Jeffra Schaffer for helping with the
604 cell cultures and insightful discussions.

605

606

607

608

609

610

611

612

613

614

615

616

617

618

619

620

621

622

623

624

625

626

627 **References**

628

- 629 1. Mergler, D.; Anderson, H. A.; Chan, L. H. M.; Mahaffey, K. R.; Murray, M.; Sakamoto, M.;
630 Stern, A. H.; Methylmercury exposure and health effects in humans: A worldwide concern.
631 *Ambio: J. Human Environ.*, **36**, 3-11 (2007)
- 632 2. Morel F.M.M.; Kraepiel, A.M.L.; Amyot, M.; The chemical cycle and bioaccumulation of
633 mercury, *Annu. Rev. Ecol. Syst.*, **29**, 543-566 (1998)
- 634 3. Barkay, T., & Schaefer, J.; Metal and radionuclide bioremediation: issues, considerations and
635 potentials. *Current opinion in microbiology*, **4**(3), 318-323. (2001)
- 636 4. Martell, A. E., & Smith, R. M. *Critical stability constants* (Vol. 1, p. 135). New York:
637 Plenum Press. (1974).
638
- 639 5. Carty, A. J., & Malone, S. F.,. The chemistry of mercury in biological systems. *The*
640 *biogeochemistry of mercury in the environment*, **3**, 433-479. (1979)
641
- 642 6. Xia K., Skyllberg U.L., Bleam W.F., Bloor P.R., Nater E.A., Helmke P.A., X-ray absorption
643 spectroscopic evidence for the complexation of Hg(II) by reduced sulfur in soil humic
644 substances, *Environ. Sci. Technol.*, **33**, 257-261 (1999)
645
- 646 7. Haitzer M., Aiken G.R., Ryan J.N., Binding of Hg(II) to dissolved organic matter: The role
647 of the mercury-to-DOM concentration ratio, *Environ. Sci. Technol.*, **36**, 3564-3570 (2002)
648
- 649 8. Khwaja, A. R., P. R. Bloom, and P. L. Brezonik, Binding constants of divalent mercury
650 (Hg^{2+}) in soil humic acids and soil organic matter, *Environ. Sci. Technol.*, **40**, 844– 849,
651 (2006)
652
- 653 9. Skyllberg, U., J. Qian, and W. Frech, Bonding of methyl mercury to thiol groups in soil and
654 aquatic organic matter, *Phys. Scr.*, **T115**, 894– 896 (2005)
655
- 656 10. Skyllberg Ulf, Competition among thiols and inorganic sulfides and polysulfides for Hg and
657 MeHg in wetland soils and sediments under suboxic conditions: Illumination of controversies
658 and implications for MeHg net production, *J. of Geophys. Res.*, **113**, (2008)
659
- 660 11. Nagy, K. L., Manceau, A., Gasper, J. D., Ryan, J. N., & Aiken, G. R., Metallothionein-like
661 multinuclear clusters of mercury (II) and sulfur in peat. *Environmental science & technology*,
662 **45**, 7298-7306. (2011)
663
- 664 12. Hesterberg, D., Chou, J.W., Hutchison, K.J., Sayers, D.E., Bonding of Hg(II) to reduced
665 organic sulfur in humic acid as affected by S/Hg ratio, *Environ. Sci. Technol.*, **35**, 2741 –
666 2745 (2001)
667
- 668 13. Loux, N., An assessment of mercury-species-dependent binding with natural organic carbon,
669 *Chemical Speciation and Bioavailability*, **10**, 127-136 (1998)

- 670
671 14. Ravichandran, M., Interactions between mercury and dissolved organic matter – a review,
672 *Chemosphere*, **55**, 319-331 (2004)
673
- 674 15. Skyllberg U., Bloom P.R., Qian J., Lin C.M., Bleam W.F., Complexation of mercury(II) in
675 soil organic matter: EXAFS evidence for linear two-coordination with reduced sulfur groups,
676 *Environ. Sci. Technol.*, **40**, 4174-4180 (2006)
677
- 678 16. Schaefer Jeffra and Morel Francois, High methylation rates of mercury bound to cysteine by
679 *Geobacter sulfurreducens*, *Nature Geoscience*, **2** (2009)
680
- 681 17. Schaefer, J. K., Rocks, S. S., Zheng, W., Liang, L. Y., Gu, B. H., Morel, F. M. M., Active
682 transport, substrate specificity, and methylation of Hg(II) in anaerobic bacteria. *Proc.*
683 *Natl. Acad. Sci.*, **108**, 8714–8719 (2011)
684
- 685 18. Thomas, S.A., Tong, T. and Gaillard, J.F., Hg (II) bacterial biouptake: the role of
686 anthropogenic and biogenic ligands present in solution and spectroscopic evidence of ligand
687 exchange reactions at the cell surface. *Metallomics: integrated biometal science*, **6**(12), 2213-
688 2222 (2014)
689
- 690 19. Lin, H., Lu, X., Liang, L. and Gu, B., Cysteine inhibits mercury methylation by *Geobacter*
691 *sulfurreducens* PCA. *Environmental Science and Technology Letters*, **2**(5) (2005)
692
- 693 20. Mishra, B., O’Loughlin, E. J., Boyanov, M., Kemner K.M., Binding of Hg(II) to high-affinity
694 sites on bacteria inhibits reduction to Hg(0) by mixed Fe(II/III) phases *Environ. Sci. Technol.*
695 **45**, 9597-9603 (2011)
696
- 697 21. Colombo M.J., Ha J., Reinfelder J.R., Barkay T., Yee N., Anaerobic oxidation of Hg(0) and
698 methylmercury formation by *Desulfovibrio desulfuricans* ND132. *Geochimica et*
699 *Cosmochimica Acta* **112**, 166-177 (2013)
700
- 701 22. Hu, H., Lin, H., Zheng, W., Rao, B., Feng, X., Liang, L., Elias, D. A., and Gu, B., Mercury
702 Reduction and Cell-Surface Adsorption by *Geobacter sulfurreducens* PCA, *Environ. Sci.*
703 *Technol.*, **47**, 10922-10930 (2013)
704
- 705 23. Graham, A. M., Bullock, A. L., Maizel, A. C., Elias, D. A., and Gilmour, C. C., Detailed
706 Assessment of the Kinetics of Hg-Cell Association, Hg Methylation, and Methylmercury
707 Degradation in Several *Desulfovibrio* Species, *Appl. Environ. Microbiol.*, **78**, 7337-7346
708 (2012)
709
- 710 24. Gu, B., Bian, Y., Miller, C.L., Dong, W., Jiang, X., Liang, L., Mercury reduction and
711 complexation by natural organic matter in anoxic environments, *Proc. Nation. Acad. Sci.*,
712 **108**, 1479-1483 (2011)
- 713 25. Zheng, W., Liang, L., Gu, B., Mercury Reduction and Oxidation by Reduced Natural
714 Organic Matter in Anoxic Environments. *Environ. Sci. Technol.* **46**, 292–299. (2012)
715

- 716 26. Colombo M.J., Ha J., Reinfelder J.R., Barkay T., Yee N., Oxidation of Hg(0) to Hg(II) by
717 Diverse Anaerobic Bacteria, *Chemical Geology*, **363**, 334-340 (2014)
- 718 27. Thomas, S.A. and Gaillard, J.F., Probing changes in Hg (II) coordination during its bacterial
719 uptake. In *Journal of Physics: Conference Series* **712**(1), 12078-12081 (2016)
720
- 721 28. Borrok D., Aumend K. and Fein J. B., Significance of ternary bacteria-metall natural organic
722 matter complexes determined through experimentation and chemical equilibrium modeling.
723 *Chemical Geology*. **238**. 44-62 (2007)
- 724 29. Lovely, D.R. and Phillips, E.J.P., Novel mode of microbial energy metabolism: organic
725 carbon oxidation coupled to dissimilatory reduction of iron or manganese. *Applied and*
726 *Environmental Microbiology*. **54**. 1472-1480 (1988)
- 727 30. Fowle, D., and Fein, J.B. Experimental measurements of the reversibility of metal-bacteria
728 adsorption reactions. *Chemical Geology*, **168**, 27-36 (2000)
- 729 31. Boyanov, M. I., S. D. Kelly, K. M. Kemner, B. A. Bunker, J. B. Fein, and D. A. Fowle. "Adsorption
730 of cadmium to Bacillus subtilis bacterial cell walls: a pH-dependent X-ray absorption fine structure
731 spectroscopy study." *Geochimica et Cosmochimica Acta* 67, no. 18 (2003): 3299-3311.
- 732 32. Claessens, Jacqueline, and Philippe Van Cappellen. "Competitive binding of Cu²⁺ and Zn²⁺ to live
733 cells of Shewanella putrefaciens." *Environmental science & technology* 41, no. 3 (2007): 909-914.
734
- 735 33. Wei, Xing, Linchuan Fang, Peng Cai, Qiaoyun Huang, Hao Chen, Wei Liang, and Xinming Rong.
736 "Influence of extracellular polymeric substances (EPS) on Cd adsorption by bacteria." *Environmental*
737 *Pollution* 159, no. 5 (2011): 1369-1374.
738
- 739 34. Segre, C.U., Leyarovska, N.E., Chapman, L.D., Lavender, W.M., Plag, P.W., King, A.S.,
740 Kropf, A.J., Bunker, B.A., Kemner, K.M., Dutta, P. and Duran, R.S., The MRCAT insertion
741 device beamline at the Advanced Photon Source. In *AIP Conference Proceedings*, **521**(1)
742 419-422 (2000).
- 743 35. Pasakarnis, T.S., Boyanov, M.I., Kemner, K.M., Mishra, B., O'Loughlin, E.J., Parkin, G. and
744 Scherer, M.M., Influence of chloride and Fe (II) content on the reduction of Hg (II) by
745 magnetite. *Environmental science & technology*, **47**(13), 6987-6994 (2013)
- 746
- 747 36. Dunham-Cheatham, S., Mishra, B., Myneni, S. C. B., Fein, J. B., The effect of natural
748 organic matter on the adsorption of mercury to bacterial cells", *Geochimica et Cosmochimica*
749 *Acta*, **150**, 1-10 (2015)
750
- 751 37. Dunham-Cheatham, S., Farrell, B., Mishra, B., Myneni, S., Fein, J. B., The effect of chloride
752 on the adsorption of Hg onto three bacterial species", *Chemical Geology*, **373**, 106-114
753 (2014)
754
- 755 38 Joe-Wong C., Shoenfelt E., Jayne E., Crompton N., Myneni SCB. Determination of organic
756 thiols in dissolved organic molecules and in bacterial cell membranes. *Environ. Sci. Technol.*,
757 **46**, 9854-9861 (2012)

- 758
759 39. Yu, Q., Szymanowski, J., Myneni, S.C.B., and Fein, J.B., Characterization of sulfhydryl sites
760 within bacterial cell envelopes using selective site-blocking and potentiometric titrations. *Chemical*
761 *Geology*, **373**, 50-58.(2014)
762
763 40. Warner, T., and Jalilehvand, F., Formation of Hg (II) tetrathiolate complexes with cysteine at
764 neutral pH. *Canadian journal of chemistry* **94**(4), 373-379 (2016)
765
766 41. Stern, E. A.; Newville, M.; Ravel, B.; Yacoby, Y.; Haskel, D. The UWXAFS analysis
767 package - philosophy and details. *Phys. B*, **209**, 117–120 (1995)
768
769 42. Harris, H. H., Pickering, I. J., George, G. N., The Chemical Form of Mercury in Fish,
770 *Science*, **301**, 1203 (2003)
771
772 43. Ravel, B.; Newville, M. ATHENA, ARTEMIS, HEPHAESTUS: Data analysis for x-ray
773 absorption spectroscopy using IFEFFIT. *J. Synchrotron Radiat.* **12**, 537–541 (2005)
774
775 44. Richens, D. T., *The Chemistry of Aqua Ions*; Wiley: Chichester, (1997)
776
777 45. Almann, R., Structure of mercuric acetate, *Z. Kristallogr., Kristallgeom., Kristallphys.,*
778 *Kristallchem.* **138**: 366–373 (1973)
779
780 46. Manceau, A., and Nagy, K.L., Relationships between Hg(II)-S bond distance and Hg(II)
781 coordination in thiolates, *Dalton Transactions*, **11**, 1421-1425 (2008)
782
783 47. Cheesman, B.V., Arnold, A.P. and Rabenstein, D.L., Nuclear magnetic resonance studies of
784 the solution chemistry of metal complexes. 25. Hg (thiol) 3 complexes and Hg (II)-thiol ligand
785 exchange kinetics. *Journal of the American Chemical Society*, **110**(19), 6359-6364 (1998)
786
787 48. Myneni SCB, Soft X-ray spectroscopy and spectromicroscopy studies of organic molecules
788 in the environment, *Rev. in Mineral. and Geochem.*, **49**, 485-579 (2002)
789
790 49. Vairavamurthy A., Using X-ray absorption to probe sulfur oxidation states in complex
791 molecules. *Spectrochimica Acta Part A- Mol. and Biomol. Spectr.*, **54**, 2009-2017 (1998)
792
793 50. Szilagy, R.K. and Schwab, D.E., Sulfur K-edge X-ray absorption spectroscopy as an
794 experimental probe for S-nitroso proteins, *Biochem. Biophys. Res. Commun.* **330**, 60-64 (2005)
795
796 51. Mishra, B., Boyanov, M., Bunker, B.A., Kelly, S.D., Kemner, K.M. and Fein, J.B., High-and
797 low-affinity binding sites for Cd on the bacterial cell walls of *Bacillus subtilis* and *Shewanella*
798 *oneidensis*. *Geochimica et Cosmochimica Acta*, **74**(15), 4219-4233 (2010)
799
800 52. Guiné, V., Spadini, L., Sarret, G., Muris, M., Delolme, C., Gaudet, J.P. and Martins, J.M.F.,
801 Zinc sorption to three gram-negative bacteria: combined titration, modeling, and EXAFS study.
802 *Environmental science & technology*, **40**(6), pp.1806-1813 (2006)
803

804 53. Yu, Q., and Fein, J.B., The effect of metal loading on Cd adsorption onto *Shewanella*
805 *oneidensis* bacterial cell envelopes: The role of sulfhydryl sites. *Geochimica et Cosmochimica*
806 *Acta* **167**, 1-10 (2015)

807 54. Wei, J.; Saxena, A.; Song, B.; Ward, B. B.; Beveridge, T. J.; and Myneni, S. C. B.;
808 Elucidation of functional groups on Gram-positive and Gram-negative bacterial surfaces using
809 infrared spectroscopy, *Langmuir*, **20**, 11433–11442 (2004)
810

811 55. Rao, B., Simpson, C., Lin, H., Liang, L., Gu, B., Determination of thiol functional groups on
812 bacteria and natural organic matter in environmental systems, *Talanta*, **119**, 240-247 (2014)
813

814 56. Xia, K., Weesner, F., Bleam, W.F., Bloom, P.R., Skyllberg, U.I., Helmke, P.A., XANES
815 studies of oxidation states of sulfur in aquatic and soil humic substances. *Soil Sci. Soc. Amer.*
816 *Journ.*, **62**, 1240-1246 (1998)
817

818 57. Risberg, E.D., Jalilehvand, F., Leung, B.O., Pettersson, L.G.M., Sandstrom, M., Theoretical
819 and experimental sulfur K-edge X-ray absorption spectroscopic study of cysteine, cystine,
820 homocysteine, penicillamine, methionine and methionine sulfoxide, *Dalton Transactions*, **12**,
821 3542-3558 (2009)
822

823 58. Gu, B., Mishra, B., Miller, C., Wang, W., Lai, B., Brooks, S.C., Kemner, K.M. and Liang, L.,
824 X-ray fluorescence mapping of mercury on suspended mineral particles and diatoms in a
825 contaminated freshwater system. *Biogeosciences*, **11**(18), pp.5259-5267 (2014)
826

827 59. Gerbig, C. A., Kim, C. S., Stegemeier, J. P., Ryan, J. N., Aiken, G. R., Formation of
828 Nanocolloidal Metacinnabar in Mercury-DOM-Sulfide Systems, *Environ. Sci. Technol.*, **45**,
829 9180-9187 (2011)
830

831 60. Zhang, T., Kim, B., Levard, C., Reinsch, B. C., Lowry, G. V., Deshusses, M. A., and Hsu-
832 Kim, H., Methylation of Mercury by Bacteria Exposed to Dissolved, Nanoparticulate, and
833 Microparticulate Mercuric Sulfides, *Environ. Sci. Technol.*, **46**, 6950-6958 (2012)
834
835
836
837
838
839
840
841
842
843
844
845
846
847
848
849

Sample	path	N	R(\AA)	σ^2 (10^{-3}\AA^2)
Hg ²⁺	Hg-O	6.12 ± 0.65	2.30 ± 0.01	15.1 ± 3.5
HgAc	Hg-O	1.78 ± 0.32	2.06 ± 0.01	10.9 ± 0.9
	Hg-C	1.78 ^a	2.83 ± 0.01	12.8 ± 4.0
Hg-cysteine	Hg-S	1.88 ± 0.21	2.32 ± 0.01	10.5 ± 1.2
*Hg-(cysteine) ₃	Hg-S	2.82 ± 0.32	2.49 ± 0.01	13.5 ± 3.5
<i>Shewanella oneidensis</i> MR-1				
350 μM	Hg-O	1.65 ± 0.25	2.06 ± 0.01	10.8 ± 1.5
	Hg-C	1.58 ± 0.32	3.05 ± 0.02	12.0 ± 3.8
100 μM	Hg-O	1.68 ± 0.24	2.06 ± 0.01	10.5 ± 1.2
	Hg-C	1.55 ± 0.28	3.05 ± 0.02	12.5 ± 3.5
50 μM	Hg-O	1.63 ± 0.15	2.06 ^b	10.9 ^b
	Hg-C	1.52 ± 0.35	3.05 ^b	12.8 ^b
	Hg-S	0.56 ± 0.12	2.32 ^c	10.5 ^c
25 μM	Hg-S	1.32 ± 0.21	2.31 ± 0.01	10.5 ± 1.5
15 μM	Hg-S	1.88 ± 0.18	2.32 ± 0.01	10.8 ± 1.3
5.0 μM	Hg-S	1.85 ± 0.19	2.35 ± 0.01	10.2 ± 1.2
2.5 μM	Hg-S	2.21 ± 0.28	2.44 ± 0.01	15.2 ± 3.0
0.5 μM	Hg-S	2.96 ± 0.25	2.51 ± 0.01	13.4 ± 2.5
<i>Bacillus subtilis</i>				
350 μM	Hg-O	1.62 ± 0.27	2.06 ± 0.01	10.8 ± 1.5
	Hg-C	1.52 ± 0.34	3.05 ± 0.02	12.0 ± 3.8
100 μM	Hg-O	1.65 ± 0.24	2.06 ± 0.01	10.5 ± 1.2
	Hg-C	1.58 ± 0.32	3.05 ± 0.02	12.5 ± 3.5
75 μM	Hg-O	1.22 ± 0.15	2.06 ± 0.01	10.9 ± 1.0
	Hg-C	1.15 ± 0.18	3.05 ± 0.01	12.8 ± 3.2

					852
25 μ M	Hg-O	1.65 \pm 0.21	2.06 ^b	10.5 ^b	853
	Hg-C	1.82 \pm 0.30	3.05 ^b	12.8 ^b	854
	Hg-S	0.42 \pm 0.10	2.32 ^c	10.5 ^c	855
					856
15 μ M	Hg-O	1.58 \pm 0.20	2.06 ^b	10.5 ^b	857
	Hg-C	2.02 \pm 0.32	3.05 ^b	12.8 ^b	858
	Hg-S	0.61 \pm 0.12	2.32 ^c	10.5 ^c	859
5.0 μ M	Hg-S	1.80 \pm 0.20	2.32 \pm 0.01	10.2 \pm 1.2	860
2.5 μ M	Hg-S	1.95 \pm 0.28	2.33 \pm 0.01	10.5 \pm 2.0	861
0.5 μ M	Hg-S	2.26 \pm 0.30	2.45 \pm 0.01	10.9 \pm 2.5	862
					863
<i>Geobacter Sulfurreducens</i>					864
75 μ M	Hg-O	1.62 \pm 0.18	2.06 ^b	10.9 ^b	865
	Hg-C	1.80 \pm 0.21	3.05 ^b	12.8 ^b	866
	Hg-S	0.46 \pm 0.14	2.32 ^c	10.5 ^c	867
25 μ M	Hg-S	1.70 \pm 0.21	2.32 \pm 0.01	9.2 \pm 1.3	868
15 μ M	Hg-S	1.96 \pm 0.18	2.32 \pm 0.01	9.5 \pm 1.7	869
5.0 μ M	Hg-S	2.06 \pm 0.19	2.36 \pm 0.01	10.6 \pm 2.8	870
2.5 μ M	Hg-S	2.21 \pm 0.28	2.38 \pm 0.01	11.2 \pm 3.0	871
0.5 μ M	Hg-S	2.24 \pm 0.22	2.38 \pm 0.01	11.5 \pm 3.6	872
					873
*This standard is predominantly Hg-(cysteine) ₃ but also contains Hg-(cysteine) ₄					874
^a Fixed this value to be the same as O based on crystallographic data.					875
^b This was set to be equal to the HgAc standard.					876
^c This was set to be equal to the Hg-cysteine standard.					877

878

879

880

881

882

883 Table 2: Values determined using qBBR measurements for surface thiol concentrations of *B.*
884 *subtilis*, *S. oneidensis* MR-1, and *G. sulfurreducens* grown in the absence of Hg^{2+} . The error is
885 one standard deviation.
886

Bacterial species	$\mu\text{moles thiol}/$ gram (wet mass)	Number of trials	wet:dry conversion	$\mu\text{moles thiol}/$ gram (dry mass)
<i>B. subtilis</i>	24 \pm 2	4	5.1	120 \pm 10
<i>S. oneidensis</i> MR-1	49 \pm 12	3	6.0	300 \pm 70
<i>G. sulfurreducens</i>	240 \pm 80	4	4.2	1000 \pm 300

887
888
889
890
891
892
893
894
895
896
897
898
899
900
901
902
903
904
905
906
907
908

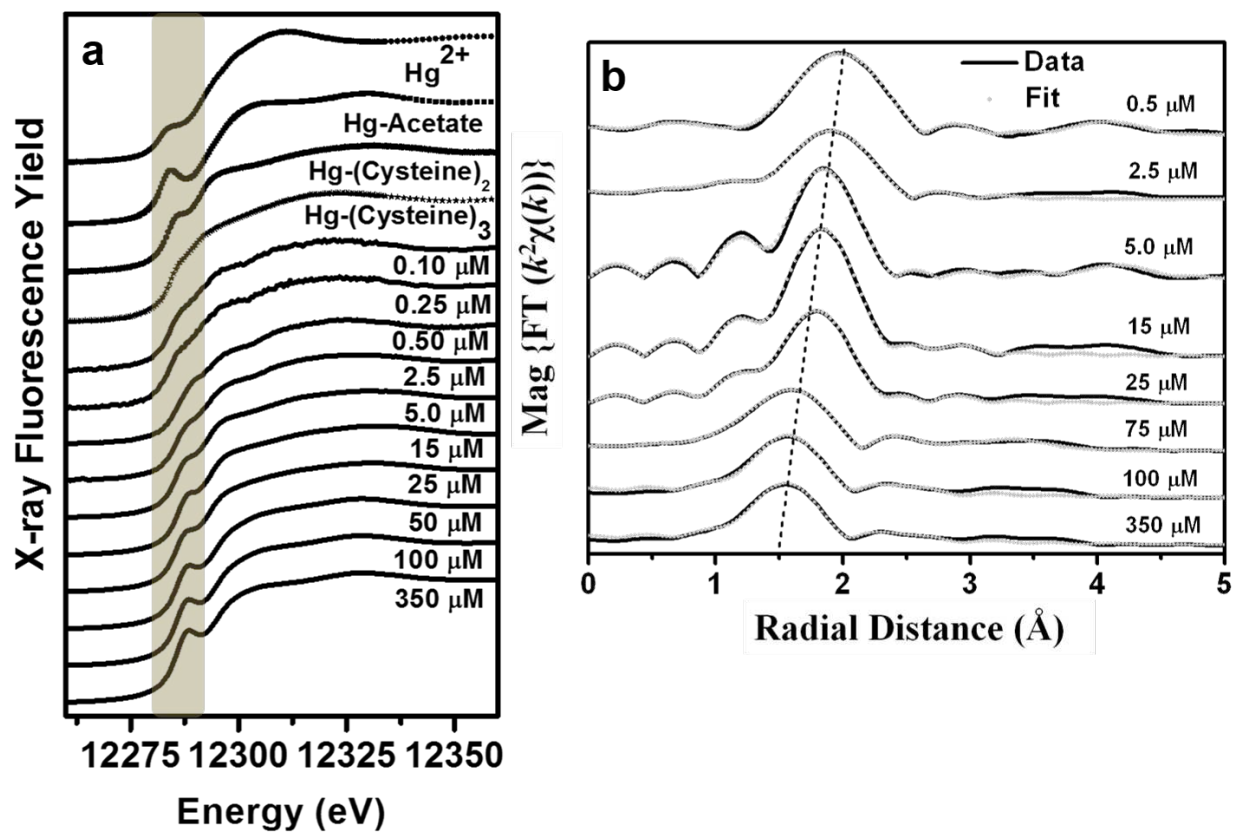
909 Table 3. Summary of surface complexation modeling results for the potentiometric titrations of
 910 *G. sulfurreducens* with and without qBBr treatment. Five replicate titrations were conducted for
 911 each condition, and the values shown here represent the averages with 1σ uncertainties.
 912

	pK_{a1}	C_1 $\mu\text{mol/g}$	pK_{a2}	C_2 $\mu\text{mol/g}$	pK_{a3}	C_3 $\mu\text{mol/g}$	pK_{a4}	C_4 $\mu\text{mol/g}$	C_{total} $\mu\text{mol/g}$
Untreated	3.2 ± 0.2	192 ± 36	5.2 ± 0.1	104 ± 7	7.2 ± 0.2	41 ± 3	9.5 ± 0.2	69 ± 20	406 ± 24
qBBr-treated	3.4 ± 0.4	139 ± 36	5.2 ± 0.1	94 ± 10	7.0 ± 0.0	44 ± 6	9.3 ± 0.1	62 ± 10	338 ± 46

913

914

915



917

918 **Figure 1.** a) Hg L_{3} -edge XANES spectra of Hg $^{2+}$ sorbed onto *S. oneidensis* MR-1 as a function
 919 of Hg $^{2+}$ concentration. XANES spectra of model Hg-organic ligand complexes are also shown
 920 for comparison. b) Fourier transform magnitude of Hg L_{III} edge EXAFS data and fits for Hg
 921 reacted *Shewanella oneidensis* MR-1.

922

923

924

925

926

927

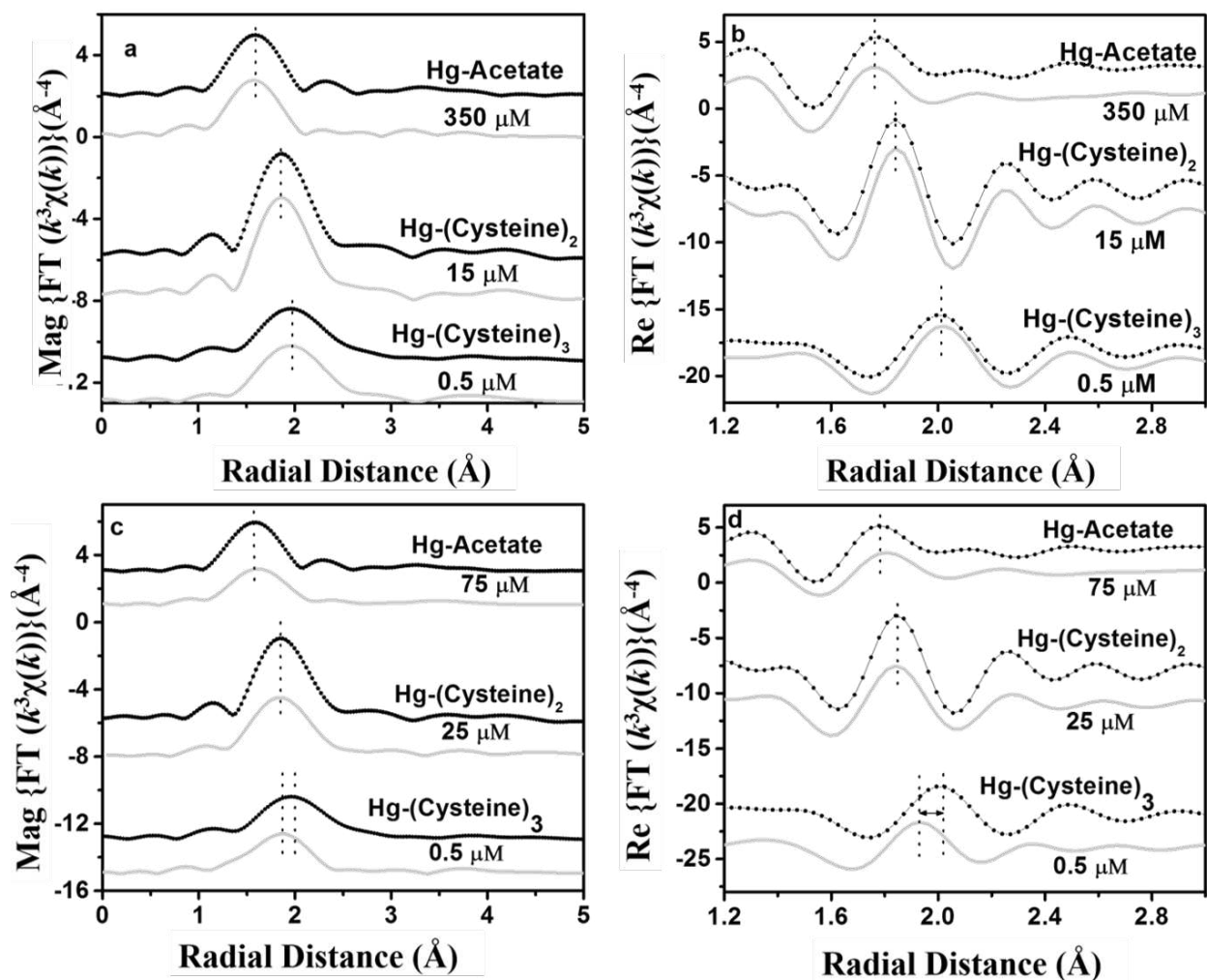
928

929

930

931

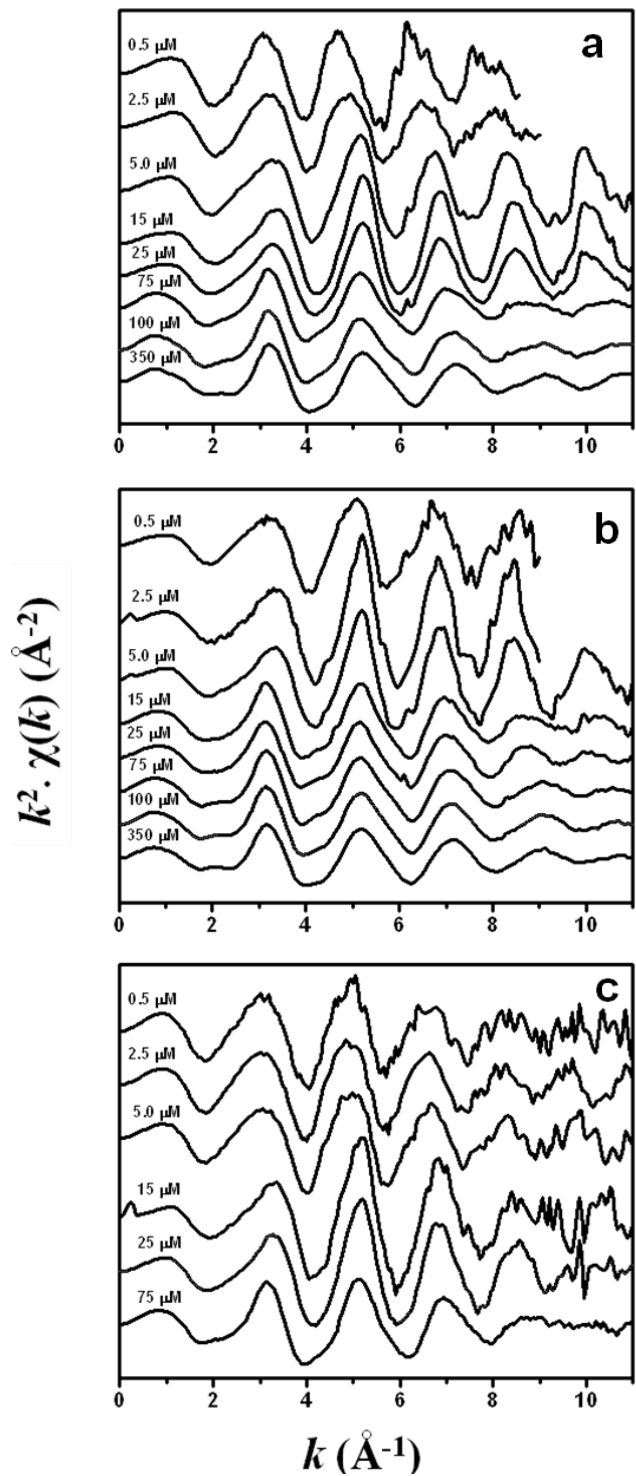
932
933
934



935
936

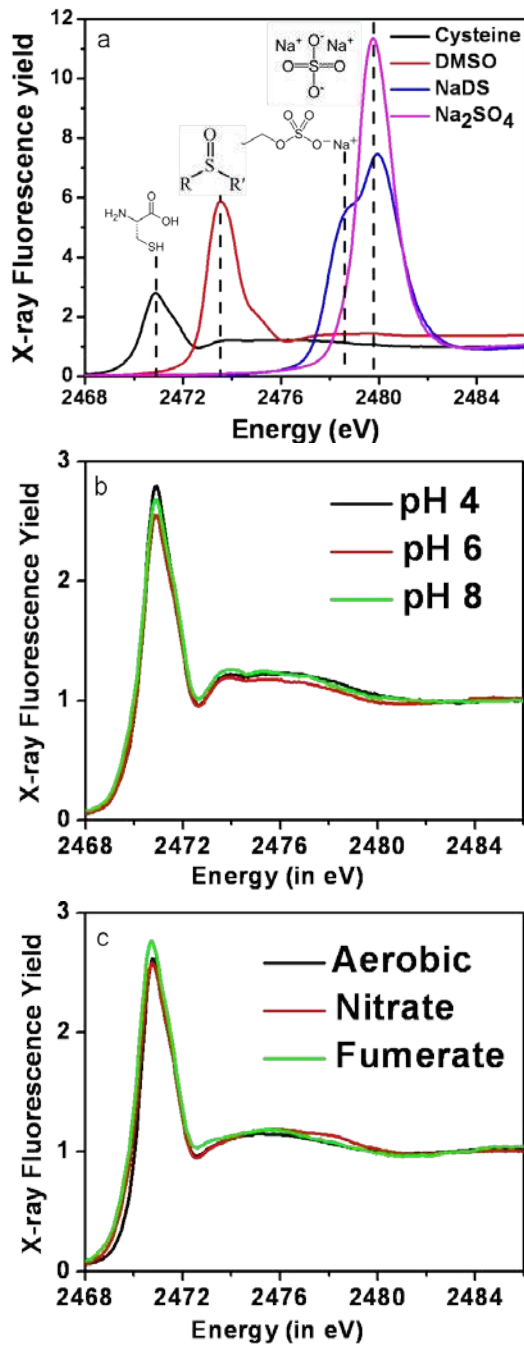
937 **Figure 2.** Structures of Hg complexes detected on cell envelopes of *S. oneidensis* MR-1 (top),
938 and *G. sulfurreducens* (bottom). The spectra in “a” and “c” correspond to the Fourier Transform
939 magnitude, and spectra in “b” and “d” correspond to the real part of Hg *L*₃ edge EXAFS spectra.
940 Spectra of Hg-carboxylate, and Hg-cysteine are also included for comparison.

941



942
 943
 944
 945
 946
 947

Figure 3: k^2 weighed $\chi(k)$ data for Hg L_{III} edge EXAFS for a) *Shewanella oneidensis* MR-1, b) *Bacillus subtilis*, and c) *Geobacter sulfurreducens*



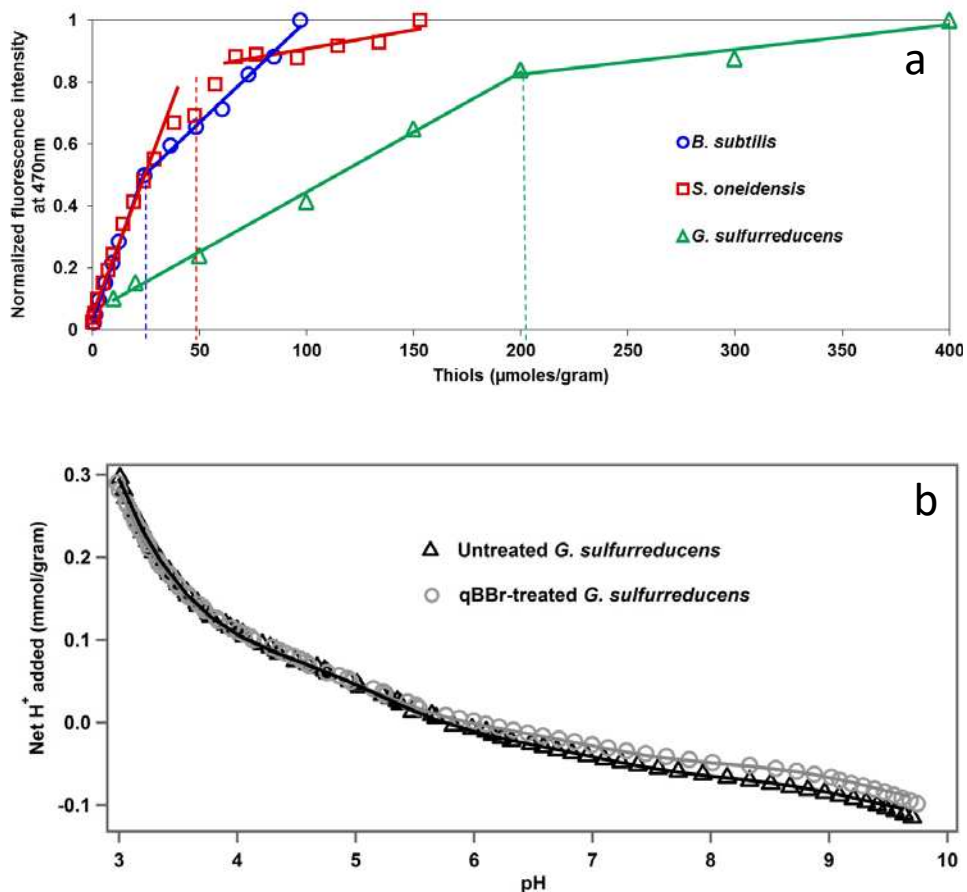
949

950

951 **Figure 4:** a) S K-edge XANES spectra of S standards (cysteine, dimethyl sulfoxide (DMSO),952 sodium dodecylsulfate (NaDS), and sodium laurel sulfate Na₂SO₄), b) S K-edge XANES on *S.*953 *oneidensis* MR-1 as a function of pH, and c) S K-edge XANES on *S. oneidensis* MR-1 cultured

954 under different conditions.

955



956

957

958 **Figure 5.** a) Concentration of reactive thiols on the cell envelopes of different bacterial species.
 959 The dashed lines indicate the saturation concentration of fluorophore (or thiol) on each cell type.
 960 b) Representative potentiometric titration curves of untreated and qBBR-treated *G.*
 961 *sulfurreducens* suspensions (10g/L). Solid curves represent the best-fitting 4-site non-
 962 electrostatic surface complexation models (SCM). Five replicate titrations were conducted both
 963 with and without qBBR treatment, and the differences in calculated total site concentrations was
 964 used to estimate the reported sulfhydryl concentrations (see Table 3).

965

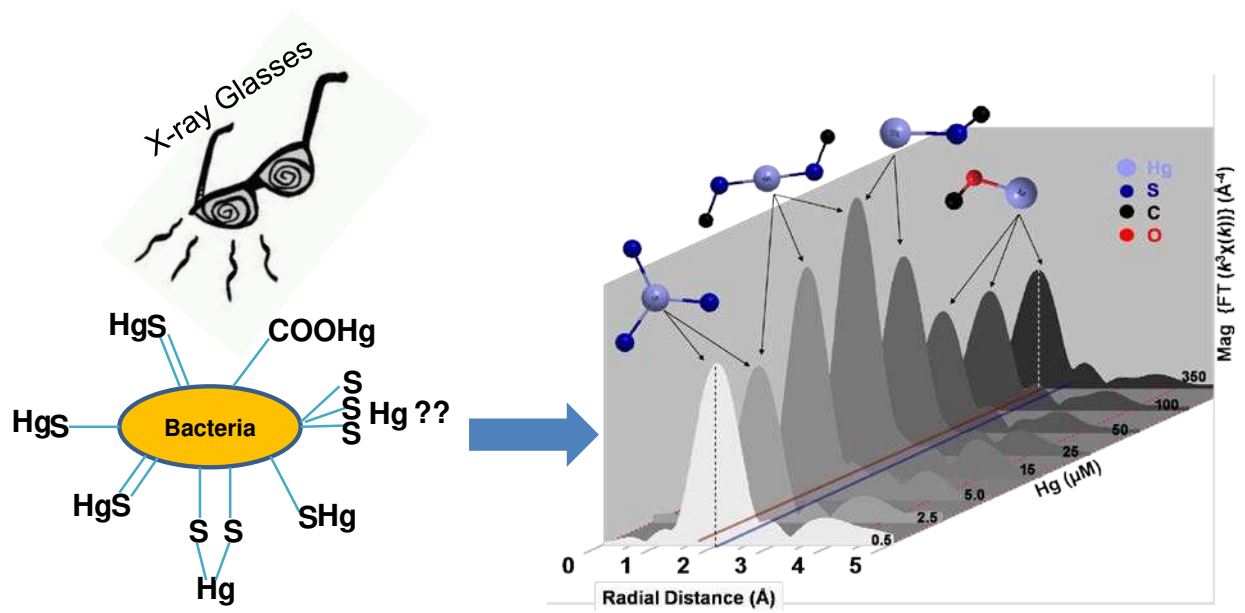
966

967

968

969

970



971

972

973

974 Artwork figure for optional graphical abstract

Supplementary Information

Stoichiometry of mercury-thiol complexes on bacterial cell envelopes

Bhoopesh Mishra^{1*†}, Elizabeth Shoenfelt², Qiang Yu³, Nathan Yee⁴,

Jeremy B. Fein³, Satish C.B. Myneni^{2*}

¹Department of Physics, Illinois Institute of Technology, Chicago, Illinois, USA

²Department of Geosciences, Princeton University, Princeton, New Jersey, USA

³Department of Civil Engineering & Geological Sciences, University of Notre Dame, Notre Dame, Indiana, USA

⁴Department of Environmental Sciences, Rutgers University, New Brunswick, New Jersey, USA

*Co-corresponding authors. Email: (bmishra3@iit.edu); (smyneni@princeton.edu)

†Present address: School of Chemical and Process Engineering, University of Leeds, Leeds, UK.

27

28 Table S1: [Hg] adsorption by biomass samples determined using ICP-OES measurements.

29

<i>B. subtilis</i>		<i>S. oneidensis</i> MR-1		<i>G. sulfurreducens</i>	
Initial Hg in solution (μM)	Hg in supernatant (μM)	Initial Hg in solution (μM)	Hg in supernatant (μM)	Initial Hg in solution (μM)	Hg in supernatant (μM)
0.04	ND*	0.06	ND*	0.05	ND*
0.11	ND*	0.14	ND*	0.15	ND*
0.21	ND*	0.20	ND*	0.24	ND*
0.43	ND*	0.45	ND*	0.52	ND*
1.07	ND*	1.12	ND*	1.2	ND*
2.15	0.10	2.10	0.08	2.76	0.12
4.26	0.15	4.55	0.12	5.20	0.21
12.93	0.21	13.10	0.18	15.01	0.45
21.49	1.26	21.60	0.62	25.23	1.16
53.32	3.58	55.7	2.86	75.54	3.085
106.36	7.80	108.3	6.52	105.82	8.42
354.03	32.76	350.03	28.45	NA	NA

30 *Not detectable.

31

32

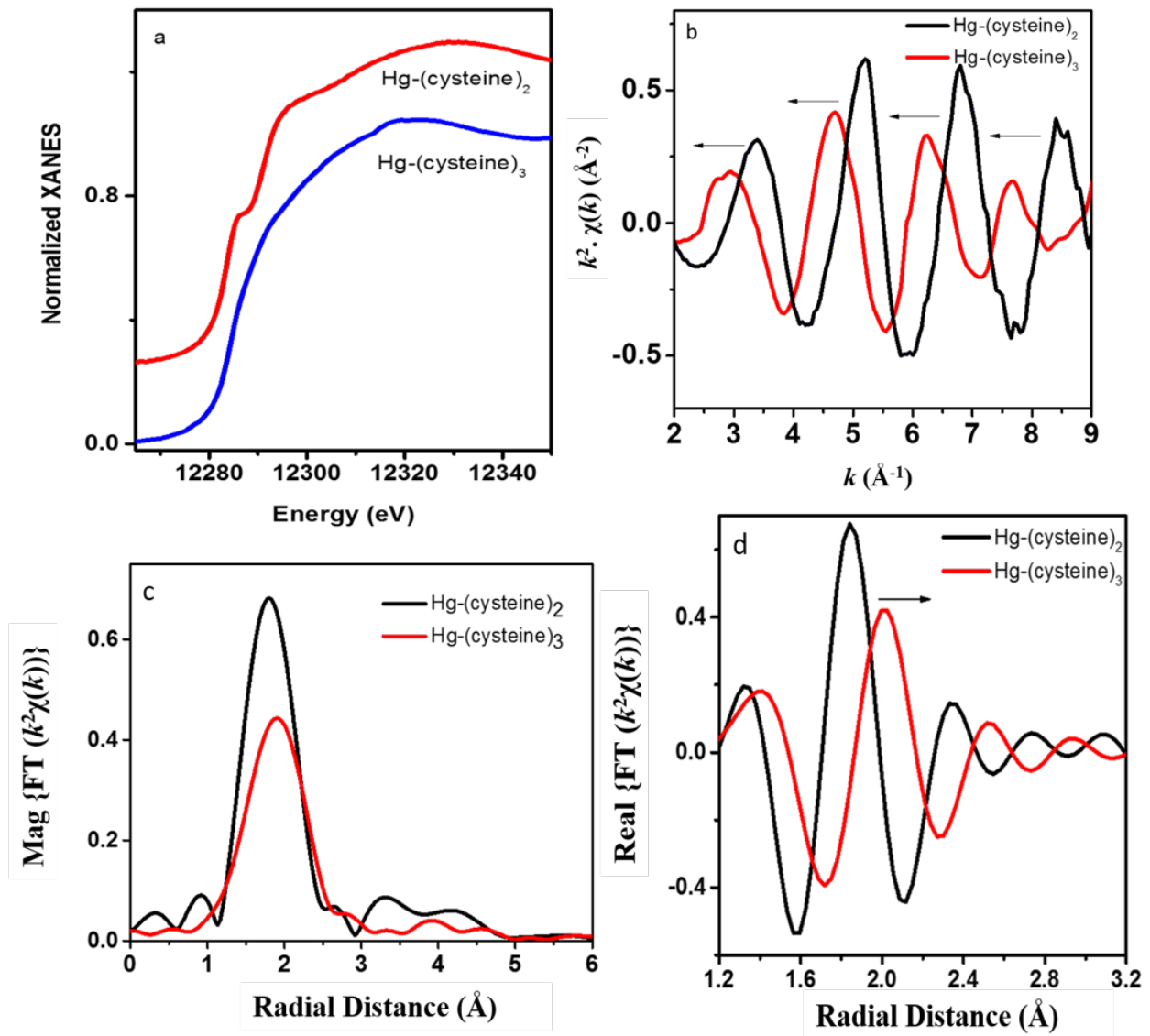
33

34

35

36

37



39

40 Figure S1: a) XANES, b) k^2 weighed $\chi(k)$ data, c) magnitude of EXAFS FT, and d) real part of
 41 the EXAFS FT data comparing Hg-(cysteine)₂ and Hg-(cysteine)₃ standards.

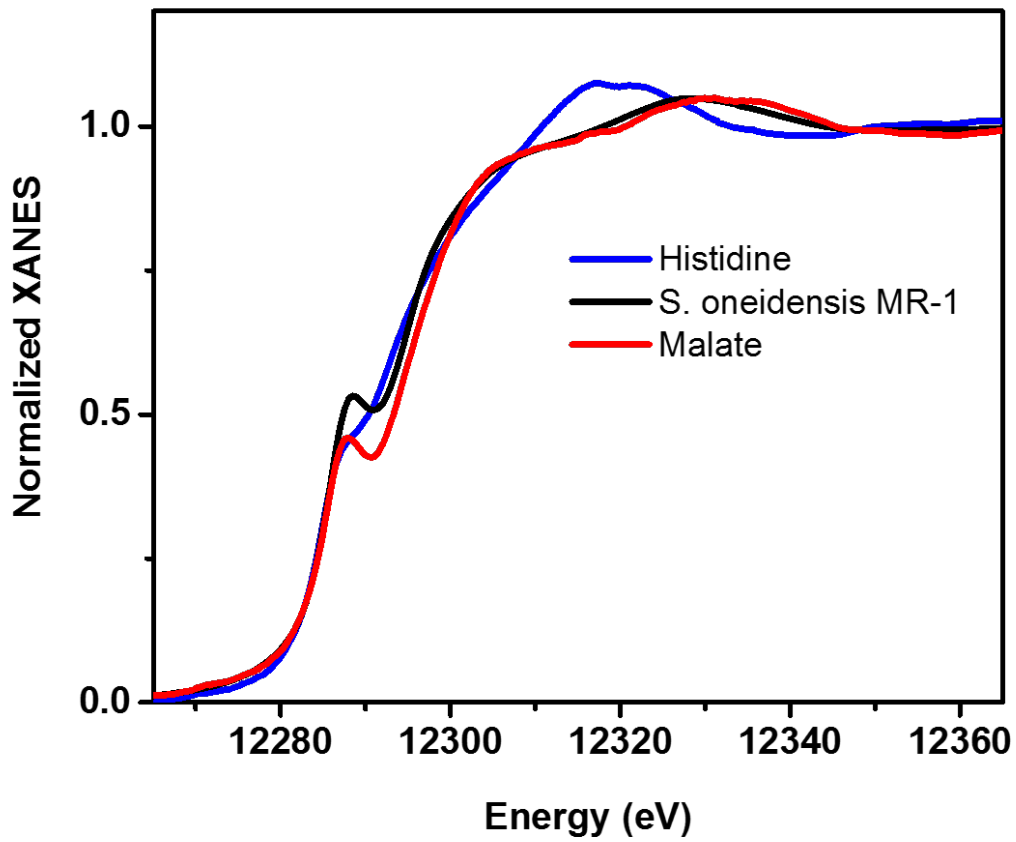
42

43

44

45

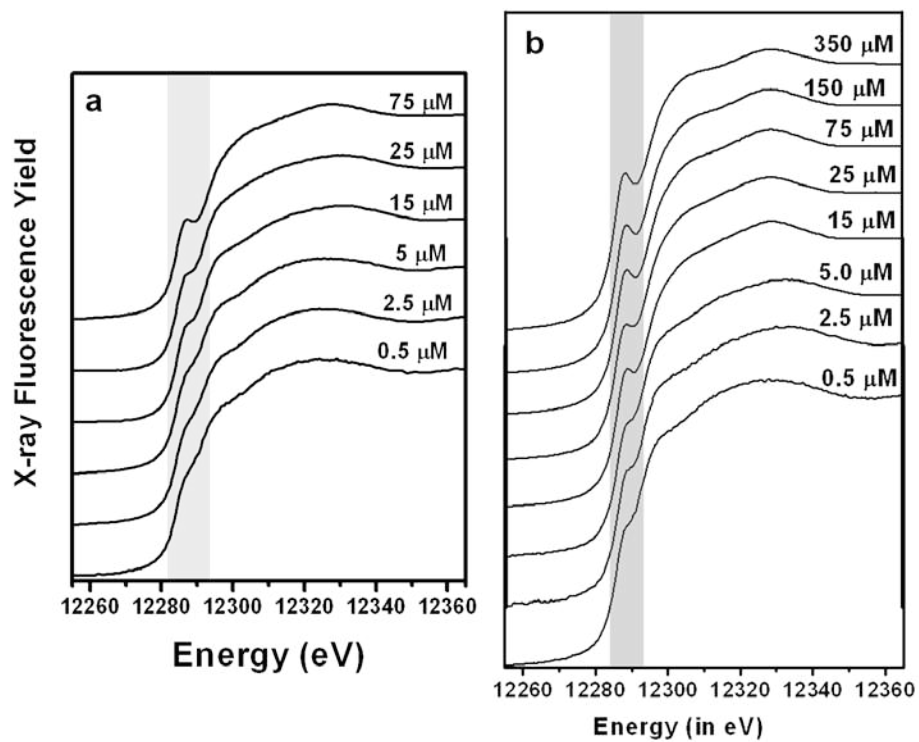
46



47

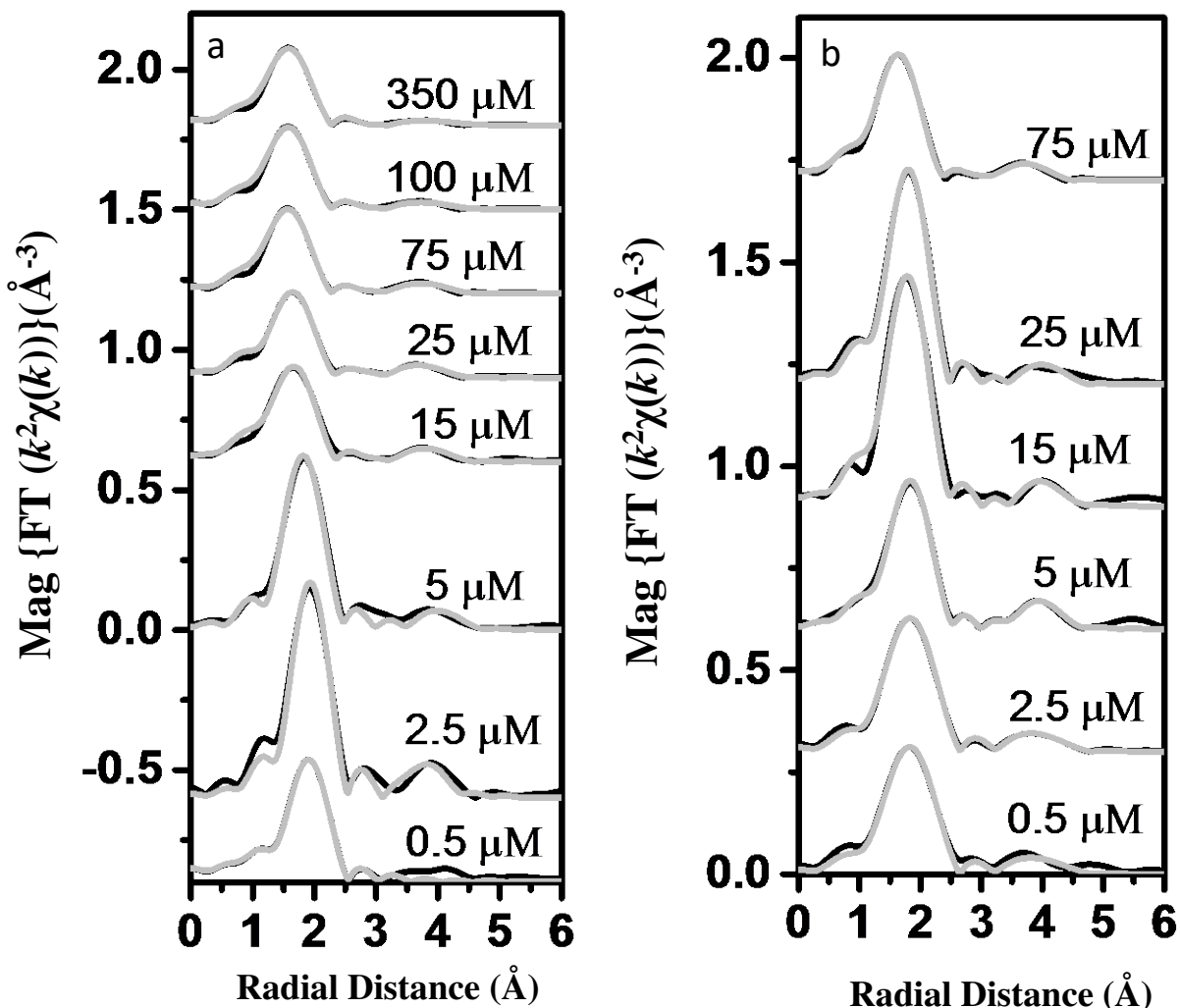
48 Figure S2: Comparison of Hg XANES spectra of Hg-histidine and Hg-malate aqueous complex
49 references with 75 μ M Hg adsorbed to *Shewanella oneidensis* MR-1 sample.

50



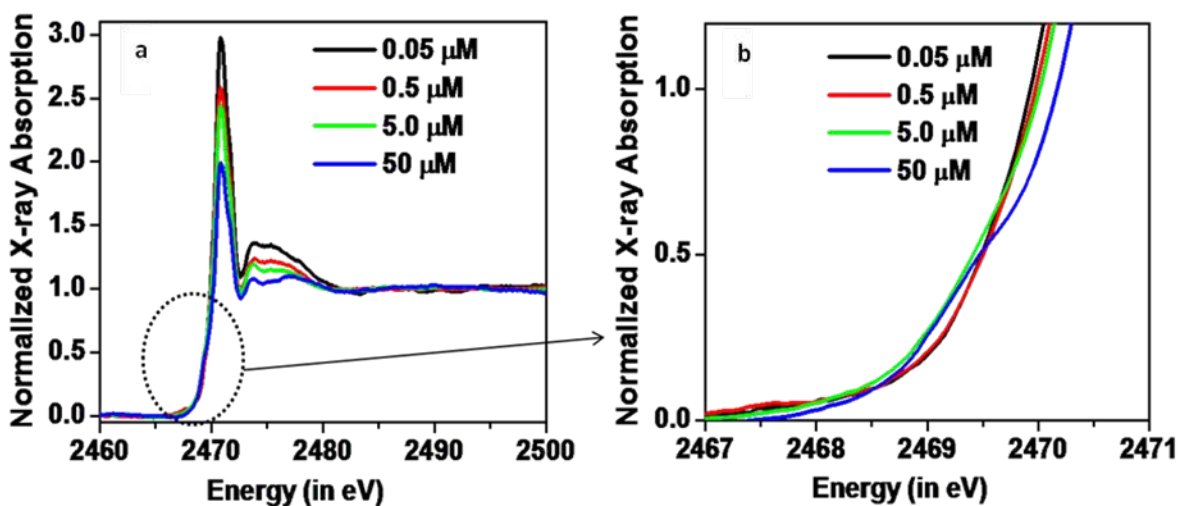
51
 52 Figure S3: a) Hg L_{III} edge XANES for Hg reacted *Geobacter sulfurreducens* and b) *Bacillus*
 53 *subtilis* biomass samples.

54
 55
 56
 57
 58
 59
 60
 61
 62
 63
 64
 65
 66
 67
 68
 69
 70
 71
 72
 73



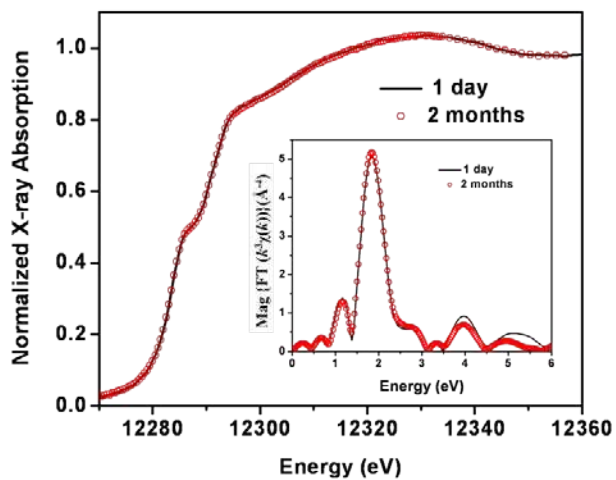
74
 75
 76
 77
 78
 79
 80
 81
 82
 83

Figure S4: a) Hg L_{III} edge EXAFS FT magnitude data (solid black line) and fit (solid light grey line) for Hg reacted *Bacillus subtilis* and b) *Geobacter sulfurreducens* biomass samples.



84
 85 Figure S5: a) S K-edge XANES spectra of *S. oneidensis* MR-1 as a function of Hg concentration,
 86 and b) expanded pre-edge region (expanded for clarity) as a function of Hg loading on *S.*
 87 *oneidensis* MR-1 indicates the deprotonation of cysteine at higher Hg loadings.

88
 89
 90
 91
 92
 93
 94
 95
 96
 97
 98
 99
 100
 101
 102



103

104 Figure S6: Hg L_{III} edge XANES on *Shewanella oneidensis* MR-1
 105 reacted with 10 μM Hg^{II} for 1 day vs. 2 months. Inset shows
 106 corresponding Fourier transformed spectra.

107

108

109

110

111

112

113

114

115

116

117

118

119

120